Systems/Circuits

Alleviating Hypertension by Selectively Targeting Angiotensin Receptor–Expressing Vagal Sensory Neurons

Caitlin Baumer-Harrison,[1,2,3,4] Khalid Elsaafien,[2,5,6] Dominique N. Johnson,[2,5,6] Jesus D. Peñaloza Aponte,[1] Alan de Araujo,[7] Sagar Patel,[1] Erin B. Bruce,[1] Scott W. Harden,[2,5] Charles J. Frazier,[2,5] Karen A. Scott,[2,5,6] Guillaume de Lartigue,[7] Eric G. Krause,[2,5,6] and Annette D. de Kloet[1,2,3,6]

[1]Department of Physiology and Aging, College of Medicine, University of Florida, Gainesville, Florida 32611, [2]Center for Integrative Cardiovascular and Metabolic Diseases, University of Florida, Gainesville, Florida 32611, [3]Center for Smell and Taste, University of Florida, Gainesville, Florida 32611, [4]Department of Psychiatry, Perelman School of Medicine, University of Pennsylvania, Philadelphia, Pennsylvania 19104, [5]Department of Pharmacodynamics, College of Pharmacy, University of Florida, Gainesville, Florida 32611, [6]Neuroscience Institute, Georgia State University, Atlanta, Georgia 30302, and [7]Monell Chemical Senses Center, Philadelphia, Pennsylvania 19104

Cardiovascular homeostasis is maintained, in part, by neural signals arising from arterial baroreceptors that apprise the brain of blood volume and pressure. Here, we test whether neurons within the nodose ganglia that express angiotensin type-1a receptors (referred to as NG^{AT1aR}) serve as baroreceptors that differentially influence blood pressure (BP) in male and female mice. Using *Agtr1a*-Cre mice and Cre-dependent AAVs to direct tdTomato to NG^{AT1aR}, neuroanatomical studies revealed that NG^{AT1aR} receive input from the aortic arch, project to the caudal nucleus of the solitary tract (NTS), and synthesize mechanosensitive ion channels, *Piezo1/2*. To evaluate the functionality of NG^{AT1aR}, we directed the fluorescent calcium indicator (GCaMP6s) or the light-sensitive channelrhodopsin-2 (ChR2) to *Agtr1a*-containing neurons. Two-photon intravital imaging in *Agtr1a*-GCaMP6s mice revealed that NG^{AT1aR} couple their firing to elevated BP, induced by phenylephrine (i.v.). Furthermore, optical excitation of NG^{AT1aR} at their soma or axon terminals within the caudal NTS of *Agtr1a*-ChR2 mice elicited robust frequency-dependent decreases in BP and heart rate, indicating that NG^{AT1aR} are sufficient to elicit appropriate compensatory responses to vascular mechanosensation. Optical excitation also elicited hypotensive and bradycardic responses in ChR2-expressing mice that were subjected to deoxycorticosterone acetate (DOCA)–salt hypertension; however, the duration of these effects was altered, suggestive of hypertension-induced impairment of the baroreflex. Similarly, increased GCaMP6s fluorescence observed after administration of phenylephrine was delayed in mice subjected to DOCA–salt or chronic delivery of angiotensin II. Collectively, these results reveal the structure and function of NG^{AT1aR} and suggest that such neurons may be exploited to discern and relieve hypertension.

Key words: autonomic; baroreceptor; baroreflex; blood pressure; nodose; vagus

Significance Statement

Hypertension is a major risk factor for cardiovascular disease and stroke, which are the first and fifth leading causes of death in the USA, respectively. Half of the adult population is afflicted with hypertension, with many not having their condition under control with current treatment options. Thus, there is a need to discover novel targets and develop new antihypertensive therapeutics. Here, we characterize the structure and function of vagal sensory neurons that express the angiotensin-II type-1a receptor (AT1aR) and provide evidence that these neurons are involved in blood pressure control. The implication is that AT1aR acts as a phenotypic marker for a subset of vagal baroreceptive neurons that may serve as a novel route to understand and alleviate hypertension.

Received June 19, 2023; revised Nov. 3, 2023; accepted Nov. 29, 2023.

Author contributions: C.B-H., K.A.S., G.L., E.G.K., and A.D.K. designed research; C.B-H., K.E., D.N.J., A.D.K., S.P., E.B.B., S.W.H., K.A.S., G.L., E.G.K., and A.D.K. performed research; C.B-H., K.E., J.D.P.A., S.W.H., C.J.F., K.A.S., G.L., E.G.K., and A.D.K. analyzed data; C.B-H. and A.D.K. wrote the paper.

This work was supported by National Institutes of Health Grants HL162540 and DC015994 to C.B-H., HL125805 and HL145028 to A.D.K., HL136595 and HL150750 to E.G.K, and American Heart Association Grant 23POST1020034 to K.E.

The authors declare no competing financial interests.

Correspondence should be addressed to Annette D. de Kloet at adekloet@gsu.edu.

https://doi.org/10.1523/JNEUROSCI.1154-23.2023

Introduction

The nervous system's ability to perceive the external and internal environments is critical for maintaining good health, especially when presented with pathological stimuli. While somatosensory modalities, like vision and taste, create the perception of the external environment, visceral afferent and humoral signals create the perception of the internal milieu. Upon receipt of these signals, the brain alters physiology and behavior in an effort to maintain

perceived homeostasis. A critical component of this interoception, with regard to cardiovascular function, is the baroreflex. Baroreceptor neurons of the petrosal and nodose ganglia (NG) detect the level of stretch imposed on the aortic arch and carotid sinus and communicate deviations to the brain (Paintal, 1973, 1977; Cunningham et al., 1995; Berthoud and Neuhuber, 2000). These neural signals then act in the nucleus of the solitary tract (NTS) to activate a reflex arc that alters autonomic outflow and adjusts cardiac output and vascular resistance to maintain blood pressure (BP) within the optimal range (Gabriel and Seller, 1970; Wehrwein and Joyner, 2013). This all occurs with remarkable temporal resolution, and the baroreflex is engaged during acute challenges (Scherrer et al., 1990; Schadt and Ludbrook, 1991; Lanfranchi and Somers, 2002). Chronic challenges to BP, like those experienced during cardiovascular disease, trigger plasticity within baroreflex circuits, and baroreflex dysfunction is considered to be requisite to the development of many forms of hypertension (Grassi et al., 2014; Mancia and Grassi, 2014). For these reasons, modulation of the baroreflex has been considered as a treatment option for hypertension for many decades (Bevegard and Shepherd, 1966; Epstein et al., 1969; Lohmeier et al., 2005; Scheffers et al., 2010; de Leeuw et al., 2015, 2017; Wallbach et al., 2020), and it is currently in clinical trials for this purpose (e.g., NCT02572024, NCT03730519, and NCT03179800).

In addition to neural (baroreflex) signals, the status of the cardiovascular system is also communicated to the brain via endocrine signals, such as those arising from the renin–angiotensin–aldosterone system (RAAS). These signals are similarly sensed by the CNS and maintain BP through a number of mechanisms (Isaacson and Reid, 1990; Fitzsimons, 1998; Morimoto et al., 2002; Li et al., 2011). Thus, endocrine and vagal afferent signals must be coordinated in order to appropriately defend cardiovascular homeostasis. Receptors for endocrine factors, such as the angiotensin type-1a receptor (*Agtr1a*, a gene encoding AT1aR), are localized to neurons of the NG (Diz et al., 1986; Speth et al., 1987; Allen et al., 1988; Diz and Ferrario, 1988; Kupari et al., 2019), thereby highlighting a potential for baroreceptor–endocrine integration to occur at the level of the peripheral sensory neuron. Based on this localization and the known influence of angiotensin II (Ang-II; the effector peptide of the RAAS) over the baroreflex and cardiovascular function, we hypothesized that *Agtr1a*-expressing neurons of the NG (referred to as NG^{AT1aR}) are involved in cardiovascular interoception. We further hypothesized that the functionality of these neurons is impacted by hypertensive stimuli including the peptide (Ang-II) itself and that these neurons may serve as a route for the development of antihypertensive therapeutics.

Here, we first use the Cre/lox system and virally mediated gene transfer, to structurally characterize the NG^{AT1aR} and determine whether sensory information pertaining to the baroreflex may be received and conveyed by these neurons. We then use optogenetics combined with telemetric evaluation of cardiovascular parameters or c-*fos* immunohistochemistry (IHC) evaluation of neural activation in cardiovascular control centers. The goal is to evaluate their cardiovascular-related function under baseline conditions, as well as the central neural circuits that are recruited by and/or contribute to the observed phenotypes. Finally, we gauge the impact of chronic elevated BP on the functionality of these neurons using in vivo calcium imaging and optogenetics. Ultimately, an important goal for this line of research is to determine whether targeting these particular neurons is effective at promoting long-term reductions in BP and thus serving as a potential therapeutic for hypertension and cardiovascular disease.

Materials and Methods

Animals. All procedures were performed at the University of Florida (Gainesville, Florida) and approved by the Institutional Animal Care and Use Committee. Male and female mice were on a C57BL/6J background, were 8–10 weeks old at the initiation of the studies, and were maintained on a 12:12 h light/dark cycle in temperature- and humidity-controlled rooms. Mice were given free access to food and water unless stated otherwise. Four different genetic models were used for this study:

1. *Agtr1a-Cre* knock-in mice (The Jackson Laboratory, stock #030553) were generated and validated as previously described (de Kloet et al., 2017).
2. *Agtr1a-tdTomato* mice were generated by breeding *Agtr1a-Cre* knock-in mice with *Ai9 stop-flox-tdTomato* mice (The Jackson Laboratory, stock #007914) to drive the expression of tdTomato in all cells expressing AT1aR.
3. *Agtr1a-ChR2* mice. *Agtr1a-Cre* knock-in mice were bred with *Ai32 stop-flox-ChR2-eYFP* mice (The Jackson Laboratory, stock #024109) to drive the expression of the light-activatable ion channel, channelrhodopsin-2 (ChR2), and eYFP in all cells that express *Agtr1a*. These *Agtr1a-ChR2* mice were used for optogenetic excitation experiments.
4. *Agtr1a-GCaMP6s* mice. *Agtr1a-Cre* knock-in mice were bred with *Ai96 stop-flox-GCaMP6s* mice (The Jackson Laboratory, stock #028866) to drive the expression of the fluorescent, slow variant calcium indicator, GCaMP6s, in all cells that express the *Agtr1a*. These *Agtr1a-Cre* × *stop-flox-GCaMP6s* mice, referred to as *Agtr1a-GCaMP6s* mice, were used for two-photon imaging experiments.

Peripheral AAV application to the NG or aortic arch. For the anterograde tracing study, one group of *Agtr1a-Cre mice* was used for the delivery of a Cre-inducible adeno-associated viral vector (AAV) into the NG using an approach that has been described previously (Han et al., 2018). Specifically, a 250 nl volume of $AAV_{PHP.S}$-FLEX-tdTomato (Addgene, catalog #28306-PHP.S), which allows for the Cre-driven expression of tdTomato, was delivered into each NG. In another group of *Agtr1a-Cre* mice, $AAV_{2/retro}$-FLEX-tdTomato (Addgene, catalog #28306-AAVrg) was delivered onto the aortic arch as previously described (Elsaafien et al., 2021). For both approaches, mice were anesthetized under isoflurane and administered analgesic (buprenorphine ER-LAB, 0.1 mg/kg, s.c.; meloxicam, 20 mg/kg, s.c.), and body temperature was maintained on a heating pad throughout the duration of the surgery. Additionally, for surgeries targeting the aortic arch, following the induction of anesthesia, animals were intubated and artificially ventilated (tidal vol, 0.2 ml; min vol, 26 ml min^{-1}; pressure, 21 cmH_2O).

Stereotaxic surgery. Some *Agtr1a-Cre* mice were used for retrograde tracing experiments, in which $AAV_{2/retro}$-FLEX-tdTomato was delivered into the caudal NTS, as previously described (Brierley et al., 2020; Mohammed et al., 2022). Other *Agtr1a-Cre* and *Agtr1a-ChR2* mice were implanted with chronic indwelling fiber optics into the caudal NTS (Mohammed et al., 2022). Briefly, 4.5 mm fiber-optic posts were implanted into the caudal NTS to allow for the delivery of optogenetic stimulation. Mice were anesthetized under isoflurane and administered analgesic (buprenorphine ER-LAB, 0.1 mg/kg, s.c.; meloxicam, 20 mg/kg, s.c.), and body temperature was maintained on a heating pad throughout the duration of the surgery. Mice were placed in a stereotax, and a midline incision was made in the skin to expose the skull surface. A hole was drilled in the skull to expose the cerebral surface, and the fiber-optic post was inserted at the following coordinates (from lambda): anteroposterior, −2.6 mm; mediolateral (ML), −0.25 mm; and (from the surface of the brain) dorsoventral, −3.5 mm. The cannula was secured in place with a skull screw and dental acrylic.

Millar catheter cardiovascular recording and acute optical stimulation. Male and female *Agtr1a-ChR2* and *Agtr1a-Cre* mice were used to evaluate the impact of acute optical stimulation of NG^{AT1aR} on BP and heart rate (HR). A Millar catheter (Model SPR1000, Millar) connected to a PowerLab signal transduction unit (ADInstruments) was used.

Mice were administered isoflurane anesthesia, and body temperature was preserved using a heating pad throughout the surgical procedure. An incision was made on the midline of the ventral neck to expose the left carotid artery. Subsequently, a segment (1 cm) of the carotid artery was separated from the vagus nerve. Using suture, the cranial end of the segment was permanently ligated, and the caudal end of the segment was temporarily occluded. Next, the carotid artery was punctured, and the catheter was inserted into the artery lumen and then secured using a suture. Finally, the NG was isolated, a 60 s baseline recording was obtained, and optical stimulation (473 nm, 10 mW, 20 ms pulse width) was delivered at 1, 5, and 15 Hz for 60 s. Data were recorded and processed using LabChart8 software (ADInstruments).

In vitro electrophysiology. To determine if optical stimulation of NG^{AT1aR} afferents into the caudal NTS induces glutamate release, in vitro voltage-clamp electrophysiological recordings were performed on *Agtr1a-ChR2* mice. Mice were anesthetized with ketamine HCl (0.1 ml of 100 mg/ml, i.p.) and decapitated, and brains were rapidly extracted. Brains were submerged in ice-cold sucrose-laden artificial cerebrospinal fluid (aCSF) containing (in mM) 205 sucrose, 10 dextrose, 1 $MgSO_4$, 2 KCl, 1.25 NaH_2PO_4, 1 $CaCl_2$, and 25 $NaHCO_3$ and oxygenated with 95% O_2/5% CO_2. A Leica VT1000 vibratome was used to prepare 300 µm horizontal sections through the NTS. Slices were then transferred to a low-calcium high-magnesium aCSF containing (in mM) 124 NaCl, 10 dextrose, 3 $MgSO_4$, 2.5 KCl, 1.23 NaH_2PO_4, 1 $CaCl_2$, and 25 $NaHCO_3$, oxygenated with 95% O_2/5% CO_2, and maintained at 37°C for 30 min. Slices were then permitted to passively equilibrate to room temperature for at least 1 h before recording. Experiments were performed with aCSF containing (in mM) 126 NaCl, 11 dextrose, 1.5 $MgSO_4$, 3 KCl, 1.2 NaH_2PO_4, 2.4 $CaCl_2$, and 25 $NaHCO_3$, oxygenated with 95% O_2/5% CO_2, and maintained at 30°C. Electrophysiological recordings were made using a MultiClamp 700B amplifier, Digidata 1440 A digitizer, and pCLAMP 11 software (Axon Instruments/Molecular Devices). Slice imaging was performed using an Olympus BX51WI upright microscope. Patch pipettes were prepared from borosilicate capillary glass (BF150-86-10) using a Flaming-Brown P97 puller (Sutter Instrument) and had an open-tip resistance of 4–6 MΩ. Pipettes were filled with an internal solution containing (in mM) 125 K-gluconate, 10 phosphocreatine, 1 $MgCl_2$, 10 HEPES, 0.1 EGTA, 2 Na_2ATP, and 0.25 Na_3GTP, adjusted to pH 7.25 and 295 mOsm. Data were recorded at 20 kHz, low-pass filtered at 2 kHz, and are presented uncorrected for liquid junction potential. Optical activation of ChR2 was achieved using a TTL-controlled light source (X-Cite 110LED, Excelitas Technologies) configured to deliver 1–10 ms light pulses through an XF404 filter cube (Omega Optical) and 40× water immersion lens.

Telemetric cardiovascular recording. For studies that evaluate cardiovascular function in awake freely moving mice, mice were implanted with radiotelemetry devices (Mohammed et al., 2022). Mice were anesthetized under isoflurane and administered analgesic (buprenorphine ER-LAB, 0.1 mg/kg, s.c.; meloxicam, 20 mg/kg, s.c.), and body temperature was maintained on a heating pad throughout the duration of the surgery. Radiotelemetry transmitters (HDX10; Data Sciences International) were placed intraperitoneally and secured to the abdominal wall using a suture. The abdominal muscles were then closed with an absorbable suture. Using the same procedure as for insertion of the Millar catheter, the fluid-filled catheter was inserted into the distal left carotid artery and secured in place with a suture. The skin was closed with a nonabsorbable 5-0 monofilament suture. During cardiovascular recordings, mice were housed in cages placed on PhysioTel receivers (Data Sciences International). To initiate data collection, we turned the devices on by touching the animal with a magnet, immediately transmitting the signal. Data were continuously acquired in 1 min bins using the Ponemah Software (Data Sciences International) for the duration of the experiment. Devices obtained recordings of systolic blood pressure (SBP), diastolic blood pressure (DBP), mean arterial pressure (MAP), and HR.

Optical stimulation in conscious freely moving mice. Agtr1a-ChR2 and *Agtr1a-Cre* mice implanted with radiotelemetry devices were subjected to optical stimulation delivered during the light cycle (~11:00 A.M.) using blue laser light (473 nm, 10 mW, 20 ms pulse width) applied at various frequencies and total time durations (1 Hz, 120 min; 2 Hz, 60 min; 3 Hz, 30 min). Importantly, for each of these stimulation paradigms, blue light pulses were administered in 2 min intervals that consisted of 1 min of pulses (1–3 Hz), followed by 1 min of rest for the entire 30–120 min duration of the stimulation protocol. In the days prior to optical stimulation, mice were habituated to being handled, tethered to a fiber-optic cable, and housed in home cages that are designed to allow for chronic tethering to fiberoptics. On the mornings of stimulation, mice were tethered to a fiber-optic attached to a laser at least 90 min prior to the delivery of optical stimulation. Throughout this paradigm, cardiovascular parameters were recorded as described above.

Some *Agtr1a-ChR2* and *Agtr1a-Cre* mice were also used for c-*fos* experiments, in which c-*fos* was induced by acute optical stimulation. To prevent increased stress, mice were tethered to a fiber-optic cable attached to a laser at least 90 min prior to the delivery of optical stimulation. Mice were then delivered blue laser light at 2 Hz for 60 min, using the intervals described above, and killed 90 min after the onset of optical stimulation as described below in the "Euthanasia and tissue preparation" section.

Chronic BP elevation using DOCA–salt or Ang-II infusion. In order to elevate BP, mice were either administered DOCA (100 mg pellet, s.c.; 60 d release, Innovative Research of America) in conjunction with ad libitum access to isotonic saline drink (0.15 M NaCl) and continued access to standard drinking water (Sumners et al., 2020; Mohammed et al., 2022) or were implanted with osmotic minipumps to chronically deliver Ang-II (600 ng/kg/min). Further experimental manipulations (i.e., optogenetic stimulation; 2P intravital imaging and/or BP) were performed between 2 and 3 weeks of DOCA–salt or Ang-II administration.

Euthanasia and tissue preparation. Mice were killed by sodium pentobarbital (50 mg/kg, i.p.) and transcardially perfused with RNase-free saline followed by 4% paraformaldehyde (PFA). Left and right NG and brains were extracted and postfixed in 4% PFA briefly or for 4–6 h, respectively. NG were then transferred to RNase-free 20% sucrose in PBS, and brains were transferred to RNase-free 30% sucrose in PBS for storage at 4°C. NG were sectioned at 10 µm using a Leica CM3050 S cryostat (Leica Microsystems), frost-mounted on Superfrost Plus Gold Slides (Thermo Fisher Scientific), and allowed to air-dry on a slide warmer for 1 h. Slides were then dipped in molecular-grade ethanol and air-dried overnight at room temperature. The following day slides were stored at −20°C until in situ hybridization (ISH) and/or IHC was performed. Brains were sectioned at 25 µm for ISH or 30 µm for IHC using a Leica CM3050 S cryostat and frost-mounted on slides or stored in cryoprotectant in wells at −20°C until ISH and/or IHC was performed.

RNAscope ISH. Left and right NG sections from *Agtr1a-tdTomato mice* and brain sections from *Agtr1a-Cre* and *Agtr1a-ChR2 mice* were used for ISH. Protease pretreatment and ISH were performed using the RNAScope Multiplex Fluorescent Assay V2 (Advanced Cell Diagnostics) as per the manufacturer's instructions. All probes were purchased from Advanced Cell Diagnostics. Target probes contained double-Z oligonucleotide probe pairs that are gene-specific and decrease nonspecific binding. A probe for *Agtr1a* (*Mm-Agtr1a-01*, catalog #481161) was used to validate the expression of tdTomato in cells expressing the AT1aR in the left and right NG. Additionally, probes for *Piezo1* (*Mm-Piezo1*, catalog #400181) and *Piezo2* (*Mm-Piezo2*, catalog #400191) were used as markers for baroreceptors (Zeng et al., 2018) to investigate the colocalization with cells expressing tdTomato. For all ISH experiments, probes for Ubc (Mm-Ubc; catalog #310771) and DapB (probe-DapB; catalog #310043) were used as the positive and negative control, respectively. All probes were assigned red (excitation, 555 nm; emission, 569 nm) or far-red (excitation, 647 nm; emission, 690 ± 10 nm) as the color label to allow for the visualization of mRNA. After the ISH protocol, slides were immediately coverslipped using ProLong Gold Antifade Mountant (Thermo Fisher Scientific).

IHC. NG and hindbrains from *Agtr1a-Cre* mice injected with Cre-inducible AAVs were used for IHC studies. Prior to IHC, slides

were removed from the freezer and allowed to dry. Slides were rinsed in 50 mM KPBS and then incubated in blocking solution (2% normal donkey serum, 0.2% Triton X-100, 50 mM KPBS) for 1 h at room temperature. For NG IHC, slides were incubated in the conjugated antibody A60 mouse anti–NeuN-AlexaFluor 488 (1:1,000; MAB377X, EMD Millipore) for 2 h at room temperature. Slides were then rinsed in 50 mM KPBS, allowed to air-dry, and then coverslipped. For instances when the tdTomato signal needed to be amplified, IHC was performed on hindbrain sections, NG, and aortic arch tissue using the primary antibody rabbit anti-mCherry (1:500; PA5-34974, Thermo Fisher Scientific) and secondary antibody donkey anti-rabbit Cy3 (711-165-152) or AlexaFluor 594 (711-585-152) purchased from Jackson Immuno Research and used at a 1:500 dilution.

IHC was also used to evaluate c-*fos* expression after optical stimulation. The primary antibodies used in this study were polyclonal rabbit anti-c-*fos* (1:2,000; RPCA-c-*fos*, EnCor Biotechnology), IgY chicken anti-GFP (1:1,000; A10262, Life Technologies), and chicken anti-tyrosine hydroxylase (1:500; AB76442; Abcam). IHC was performed on brain tissue sections in wells or on slides, using a modified protocol similar to that described above. For IHC on tissue in wells, all steps were performed on a shaker at room temperature unless stated otherwise. Sections were rinsed in 50 mM KPBS to remove cryoprotectant and blocked in blocking solution (2% normal donkey serum, 0.2% Triton X-100, 50 mM KPBS) for 1 h. Sections were then incubated in the primary antibodies overnight at 4°C. To remove the primary antibodies, sections were rinsed in 50 mM KPBS and then incubated in secondary antibodies for 2 h. The secondary antibodies used in this study were donkey anti-chicken AlexaFluor 488 (703-545-155), donkey anti-chicken Cy3 (703-165-155), and donkey anti-rabbit Cy5 (711-175-152; or AlexaFluor 647, 711-605-152) and were purchased from Jackson ImmunoResearch and used at a 1:500 dilution. Finally, sections were rinsed in 50 mM KPBS and immediately mounted to slides.

Image capture and processing. Images were captured with a Nikon confocal using NIS-Elements software version 5.30.03 or an AxioImager fluorescent ApoTome microscope (Carl Zeiss) using AxioVision version 4.8.2 or Zeiss ZEN version 3.0 blue edition software. Each channel was measured, and exposure time was adjusted for optimal settings. For c-*fos* IHC, *z*-stacks were acquired at 20× magnification, unless stated otherwise, throughout the brain regions of interest (ROI) using neuroanatomical landmarks. The brain ROIs included the following: NTS, median preoptic nucleus (MnPO), paraventricular nucleus of the hypothalamus (PVN), supraoptic nucleus (SON), central nucleus of the amygdala (CeA), lateral parabrachial nucleus (LPBN), locus coeruleus (LC), rostral ventrolateral medulla (RVLM), caudal ventrolateral medulla (CVLM), nucleus ambiguus (NA), and dorsal motor nucleus of the vagus (DMNV). Exposure time for the c-*fos* channel (far-red) was kept the same for all samples within a cohort. For ISH in the NG, *z*-stacks were captured at 40× magnification. As described in detail in de Kloet et al. (2016), the exposure time was determined from sections hybridized with the positive control probe, and background fluorescence was determined from sections hybridized with the negative control probe (*DapB*) within each cohort to provide optimal visualization of the mRNA signal.

Two-photon imaging of NG. An upright two-photon microscope (Bruker Investigator) coupled with a Spectra-Physics X3 femtosecond laser was used to acquire images at ∼29 frames/s in galvo-resonant mode. The excitation wavelength was tuned to 920 nm, and a piezoelectric motor was used to rapidly step through the *z*-axis space. Control and hypertensive *Agtr1a-GCaMP6s* mice were fasted for at least 2 h before the dark onset to avoid confounding variables arising from the gut. Mice were anesthetized under isoflurane, and body temperature was maintained on a heating pad. A polyurethane cannula was inserted into the left femoral vein for the intravenous administration of phenylephrine (0.1 mg/kg). Following that, the left vagus nerve was separated from the left common carotid artery. The NG was exposed, and the rostral end of the vagus nerve was transected. The NG was then placed on an imaging platform that consisted of an 8 mm diameter coverslip attached to a metal arm affixed to a magnetic base. Surgical silicone adhesive (Kwik-Sil, World Precision Instruments) was applied onto the vagus nerve to keep it immobilized on the coverslip, and the NG was immersed in a drop of DMEM (Corning, 10-014-CV) media and then covered with a second coverslip. Imaging was performed using a 20× water immersion upright objective. A 60 s baseline was acquired followed by a 120 s recording after administration of phenylephrine. Animals were killed at the end of the experiment.

Data analysis and statistics. For cardiovascular recordings obtained from anesthetized male and female mice, SBP and HR responses in *Agtr1a-ChR2* and *Agtr1a-Cre* mice were analyzed in 1 s bins and reported relative to a 60 s baseline period. Responses to different frequencies of optical stimulation were analyzed by two-way repeated measures (RM) ANOVA or mixed-effects analysis, where appropriate, followed by Dunnett's or Tukey's multiple-comparisons tests to understand within and between effects, respectively, using Prism GraphPad Software. Cardiovascular recordings obtained from anesthetized male *Agtr1a-GCaMP6s* mice were analyzed in 30 s bins and reported relative to a baseline period. Responses to phenylephrine were analyzed by two-way RM ANOVA followed by Tukey's multiple-comparisons test.

For electrophysiological studies, responses to blue light pulses were measured in NTS neurons voltage-clamped at −50 mV. An evoked response was considered to be present if the peak current observed in a 50 ms window immediately after the light pulse was ≥5 times the root mean square (RMS) noise observed during the 50 ms immediately preceding the light pulse (referred to as the baseline period). Light-evoked current in the presence of glutamate receptor antagonists (20 μM DNQX and 40 μM AP5) is reported as the mean light-evoked response observed in a 3 min window beginning 5 min after application of the antagonists. Data were normalized to a 5 min baseline period and evaluated for significance using a one-sample *t* test (where the null hypothesis is that mean during treatment = 100%).

For telemetry recordings obtained from awake, behaving mice, data were converted and analyzed in 10 min bins and were reported as deltas relative to a 10 min baseline period. Responses to the different frequencies of optical excitation were compared at 30 min following stimulation onset using a mixed-effects analysis followed by Dunnett's (within-subjects) or Sidak's (between-subjects) multiple-comparisons tests. Time course data for all parameters were analyzed using a two-way RM ANOVA followed by Dunnett's multiple-comparisons (within-subjects) or Sidak's multiple-comparisons (between-subjects) tests using Prism GraphPad Software.

For ISH and c-*fos* IHC quantification, images were analyzed using ZEN 3.1 blue or ImageJ. Max projection images from *z*-stacks of brain ROIs and the NG were used to manually quantify c-*fos* and mRNA expression, respectively. Any adjustments to settings made for c-*fos* or ISH were kept consistent within a cohort. For evaluating the percentage of NeuN-positive and *Agtr1a*-tdTomato neurons that contain the mRNA of interest (e.g., *Agtr1a*), cells were considered to contain the mRNA if at least three visible transcripts, defined as individual puncta, were observed within the volume of NeuN or tdTomato fluorescence. c-*fos* expression was quantified by counting the number of c-*fos*–positive nuclei per section within an ROI. The mean numbers of c-*fos*–positive nuclei per section were then determined by averaging the values across sections for each individual animal and then calculating the mean across a group. Analysis of c-*fos* quantification was conducted using unpaired *t* tests with Prism GraphPad Software.

For two-photon Ca^{2+} imaging, recordings were processed using a custom Python pipeline to extract the $\Delta F/F$ Ca^{2+} traces for each neuronal component detected through our video acquisition system. First, the video was dimensionally reduced by calculating the maximum intensity projection per scanning cycle. Next, the recordings were processed using CaImAn (Giovannucci et al., 2019), a Python toolbox for large-scale Ca^{2+} imaging data. During this step, the recordings were downsampled, aligned, motion-corrected, source-separated, and deconvolved. Responses were considered if the change in fluorescence was at least 3 SD above baseline fluorescence. To further explore the activity-dependent neuronal response after phenylephrine, the recordings were separated into 60 s bins giving three phases: baseline, early post-phenylephrine onset, and late post-phenylephrine onset. The baseline represented the neuronal

activity response prior to phenylephrine administration. Early post-phenylephrine onset indicated the 60 s following phenylephrine administration. Lastly, late post-phenylephrine started 60 s after phenylephrine onset and continued for 60 s. Normalized, filtered, and presorted neuronal activity ($\Delta F/F$ Ca^{2+} traces) were analyzed in 5 s bins and statistically analyzed using the Wilcoxon rank-sum test. Each phase was compared with each other. Traces that were not statistically different from baseline and either phenylephrine onset or post-phenylephrine onset were classified as stable or nonresponders. If traces were statistically different from the baseline in either the early phase or the late post-phenylephrine onset phase, the detected neurons were classified as early or late responders. Following the Wilcoxon rank-sum test, we tested the hypothesis that phenylephrine could change the network activity response by manipulating individual neuronal activity to excitation or inhibition. This was assessed by determining the slope value between the baseline and either phase. Neurons were considered excitatory if the slope value was positive. Lastly, the aggregated $\Delta F/F$ for the groups were averaged and analyzed using Prism GraphPad Software. $\Delta F/F$ responses to phenylephrine were analyzed using two-way RM ANOVA followed by Sidak's multiple-comparisons tests to compare within and between effects. The area under curves (AUCs) were calculated from the aggregated $\Delta F/F$ from 1 to 60 s (baseline), 61 to 120 s (early post-phenylephrine), and 121 to 180 s (late post-phenylephrine) for each group and analyzed using two-way ANOVA followed by Sidak's multiple-comparisons test.

Results

Agtr1a are expressed on the vagal afferent neurons of the NG

Numerous studies have localized angiotensin receptor binding sites (Diz et al., 1986; Speth et al., 1987; Allen et al., 1988; Diz and Ferrario, 1988; Healy et al., 1989) and mRNA(s) (Bai et al., 2019; Kupari et al., 2019; Zhao et al., 2022) to vagal afferent neurons that transmit visceral sensory information to the NTS by way of the NG. Here, RNAscope ISH has similarly revealed that a subset of NG neurons (~33.9 ± 2.1%) express mRNA(s) for *Agtr1a* (Fig. 1*A–D*). Thus, we used *Agtr1a-Cre* and *Agtr1a-tdTomato* mice (i.e., *Agtr1a-Cre* X *Ai9 stop-flox-tdTomato*; Fig. 2*A*), to assess the structure of these NG^{AT1aR}. Studies in *Agtr1a-tdTomato* reporter mice revealed the presence of tdTomato afferents and soma within the NTS and NG, respectively (Fig. 2*B,C*). Further evaluation of the NG collected from these reporter mice revealed that, similar to what we have previously reported for specific brain areas [e.g., PVN (de Kloet et al., 2017)], tdTomato fluorescence faithfully colocalizes with *Agtr1a* mRNA(s) (Fig. 2*C–F*). Additionally, a substantial proportion of *Agtr1a-tdTomato* NG cells contain mRNA(s) for the mechanically gated ion channels, *Piezo1* (Fig. 2*G–J*) and *Piezo2* (Fig. 2*K–N*); these findings are consistent with a role for angiotensin-sensitive neurons in mechanosensation and, in particular, baroreceptor function (Zeng et al., 2018; Huo et al., 2021). It is important to note that a substantial proportion of these neurons do not express *Piezo1/2*, and therefore, these NG^{AT1aR} are distinct from previously studied $NG^{Piezo1/2}$ populations (Zeng et al., 2018; Min et al., 2019).

The next studies used AAV-mediated gene transfer and *Agtr1a-Cre* mice to direct tdTomato specifically to NG^{AT1aR} and clarify whether these neurons are indeed anatomically positioned to receive baroreceptor afferent signals from the vasculature and relay interoceptive information to the NTS. AAVs that direct the Cre-dependent expression of tdTomato for use as an anterograde (PHP.S serotype; applied to soma) or retrograde (AAV2/retro serotype; applied to terminals) tract tracer were applied to the components of this pathway (i.e., the NG, the caudal NTS, or the aortic arch) in separate *Agtr1a-Cre* mice (Fig. 3*A,E,I*). The fidelity of the approach was corroborated by ISH for *Agtr1a* mRNA(s) conducted on NG (84 ± 2.6% of tdTomato cells expressed *Agtr1a* mRNAs; $n = 6$ NG); and, importantly, all three routes of administration led to effective labeling of the soma of NG^{AT1aR} with tdTomato (Fig. 3*B,F,J*). Furthermore, all three routes of administration of AAV-FLEX-tdTomato revealed dense innervation within the NTS (Fig. 3*C,G,K*) and aortic arch by tdTomato-labeled fibers (Fig. 3*D,H,L*) with the latter exhibiting aortic claw-like structure that is indicative of these being baroreceptor afferents (Min et al., 2019).

Optical stimulation of the soma of NG^{AT1aR} causes robust frequency-dependent decreases in BP and HR in male and female mice

During periods of high BP, increased stretch on the vascular wall generates nerve impulses that signal to the brain the need to initiate compensatory responses that reduce cardiac output and vascular resistance to restore optimal perfusion pressure. In general, greater stretch elicits the generation of action potentials that occur at a higher frequency (Brown, 1980; Armstrong et al., 2022). Here, we hypothesized that NG^{AT1aR} are critical for these responses and that activation of NG^{AT1aR} would, therefore, be sufficient to elicit frequency-dependent reductions in BP and HR. To test this, we generated mice that express the light-sensitive cation channel, ChR2, and the reporter gene, eYFP, in all cells that contain *Agtr1a*. The approach used to generate these subjects was similar to what was used to generate *Agtr1a-tdTomato* reporter mice and required the breeding of *Agtr1a-Cre* mice with *Ai32 stop-flox-ChR2-eYFP* mice (Fig. 4*A*). In male *Agtr1a-ChR2* mice, baseline SBP was 92.98 ± 3.84 mmHg, and HR was 500.46 ± 17.68 bpm. In female

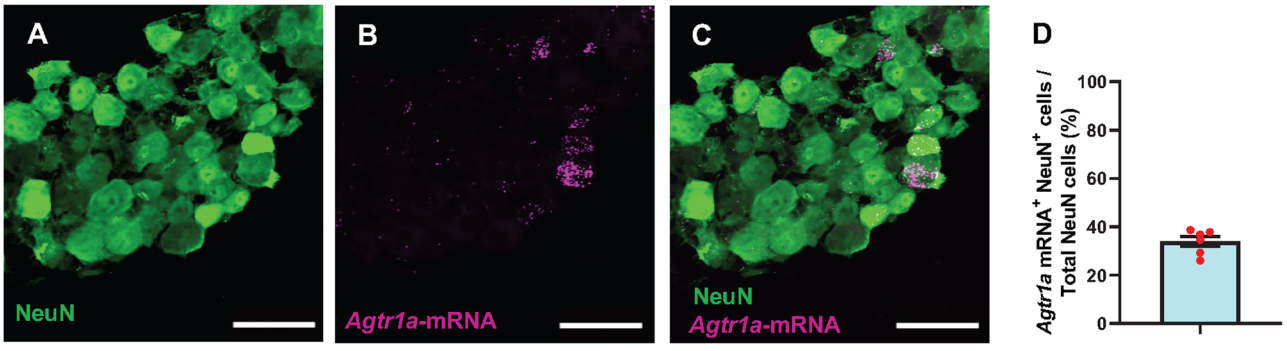

Figure 1. *Agtr1a* mRNA(s) are localized to a subset of neurons of the NG. ***A–C***, Representative images of an NG section showing (***A***) neurons labeled by NeuN (green) and (***B***) *Agtr1a* mRNA (magenta) and (***C***) the merged image depicting the localization of *Agtr1a* mRNA to NG neurons. ***D***, Quantification of the percentage of NeuN-positive NG neurons expressing *Agtr1a* mRNA ($n = 6$; error bars = SEM). Scale bar = 25 µm.

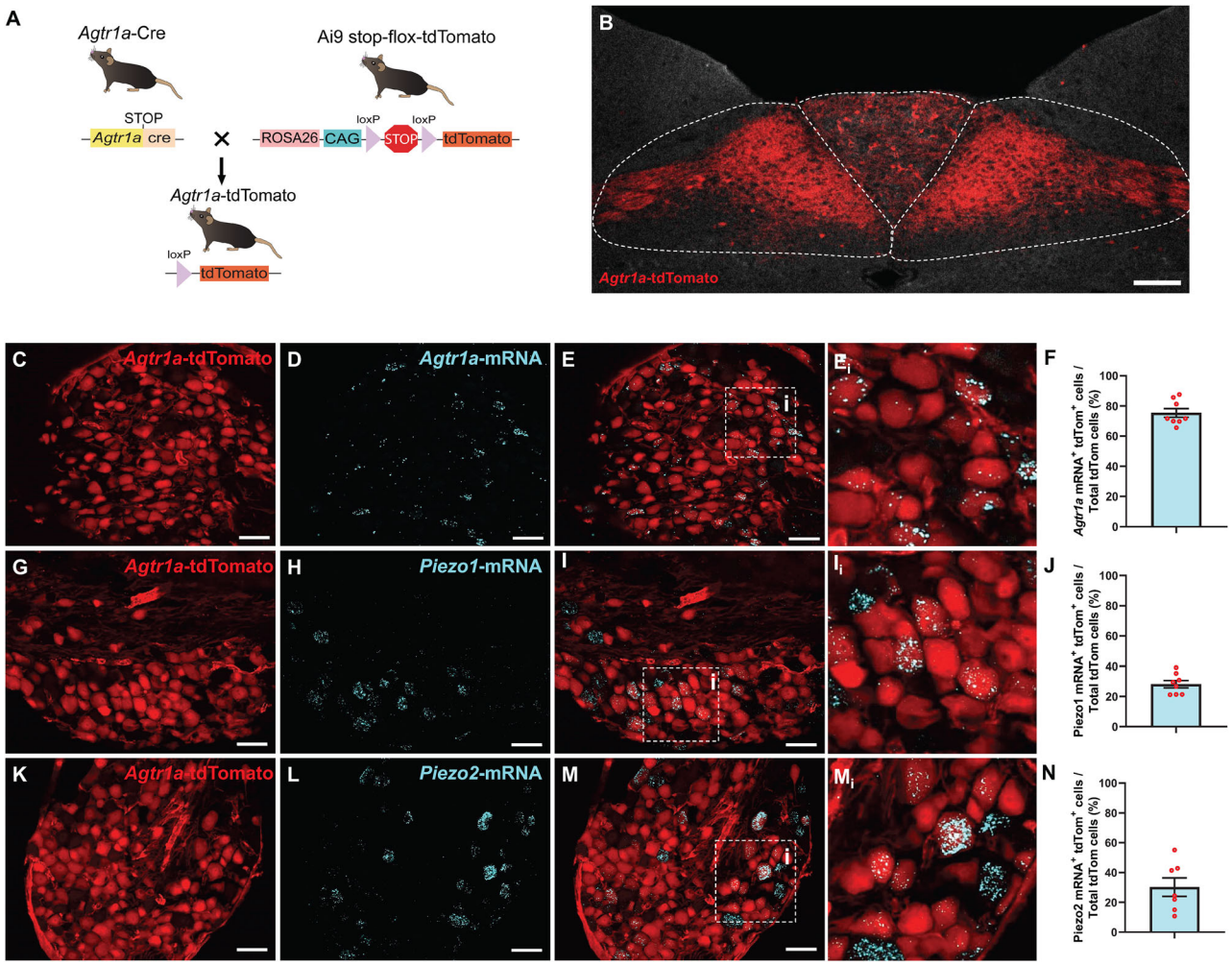

Figure 2. *Agtr1a-tdTomato* is localized to vagal afferent neurons, a subset of which expresses the mechanosensitive ion channels, *Piezo1* and *Piezo2*. ***A***, Illustration depicting the generation of the *Agtr1a-tdTomato* reporter mouse line. ***B***, Representative image (20×) of a coronal section through the caudal NTS from an *Agtr1a-tdTomato* mouse. ***C–F***, Validation of *Agtr1a* mRNA expression in the NG of *Agtr1a-tdTomato* mice. Representative images of (***C***) tdTomato expression in NG^{AT1aR} neurons (red) and (***D***) *Agtr1a* mRNA (cyan), (***E***) the merged image, and (***E$_i$***) the magnification of the merged image. ***F***, Quantification of the percentage of tdTomato-expressing neurons colocalized with *Agtr1a* mRNA ($n = 8$). Representative images of (***G***) tdTomato expression in NG^{AT1aR} neurons (red) and (***H***) *Piezo1* mRNA (cyan), (***I***) the merged image, and (***I$_i$***) the magnification of the merged image. ***J***, Quantification of the percentage of tdTomato-expressing neurons colocalized with *Piezo1* mRNA ($n = 8$). Representative images of (***K***) tdTomato expression in NG^{AT1aR} neurons (red) and (***L***) *Piezo2* mRNA (cyan), (***M***) the merged image, and (***M$_i$***) the magnification of the merged image. ***N***, Quantification of the percentage of tdTomato-expressing neurons colocalized with Piezo2 mRNA ($n = 7$). Error bars = SEM. Scale bars = 100 µm (***B***) and 25 µm (***C–M***).

Agtr1a-ChR2 mice, baseline SBP was 99.45 ± 4.78 mmHg, and HR was 433.29 ± 18.05 bpm. Acute optical stimulation of the soma of NG^{AT1aR} neurons of *Agtr1a-ChR2* mice led to robust and frequency-dependent reductions in SBP and HR (Fig. 4*B*,*C*). This phenotype was observed in both male and female mice (Fig. 4*B*,*C*). In other words, in *Agtr1a-ChR2* mice, there was a significant time–frequency interaction for SBP in both males (Fig. 4*B*; $F_{(70,490)} = 11.65$; $p < 0.0001$, two-way RM ANOVA) and females (Fig. 4*C*; $F_{(70,348)} = 11.23$; $p < 0.0001$, mixed-effects analysis). A similar interaction was also revealed for HR in males ($F_{(70,490)} = 3.03$; $p < 0.0001$, two-way RM) and females ($F_{(70,420)} = 2.47$; $p < 0.0001$, two-way RM ANOVA). Post hoc analyses (Dunnett's multiple-comparisons test) revealed that optical stimulation at 5 Hz significantly reduced SBP relative to baseline (time = 0 s) between 10 and 90 s in males and between 20 and 90 s in females (Fig. 4*B*,*C*). At 15 Hz, SBP responses were significantly different from baseline in males between 10 and 130 s and in females between 0 and 140 s (Fig. 4*C*). Additionally, optical stimulation at 5 Hz significantly reduced HR relative to baseline (time = 0 s) in females at 50 s (Fig. 4*C*). At 15 Hz, HR responses were significantly different from baseline in males between 10 and 60 s and in females between 0 and 80 s (Fig. 4*B*,*C*). Importantly, acute optical stimulation of NG^{AT1aR} neurons in control mice expressing only the *Agtr1a*-Cre gene ($n = 6$) did not have a significant effect on SBP ($F_{(72,359)} = 1.25$, $p = 0.0973$, mixed-effects analysis) or HR ($F_{(72,359)} = 1.21$, $p = 0.14$, mixed-effects analysis). The implication is that the firing of NG^{AT1aR} is indeed sufficient to simulate the enhanced perception of stretch on the vasculature, thus leading to compensatory decreases in BP and HR.

Agtr1a-containing afferent input within the NTS is sufficient to prompt cardiovascular baroreflex responses in conscious freely moving male mice

An abundance of the AT1R binding sites within the NTS arises from the NG, as unilateral ablation of the NG eliminated the binding in the ipsilateral NTS (Speth et al., 1987). Additionally, the majority of vagal afferent neurons express vesicular glutamate

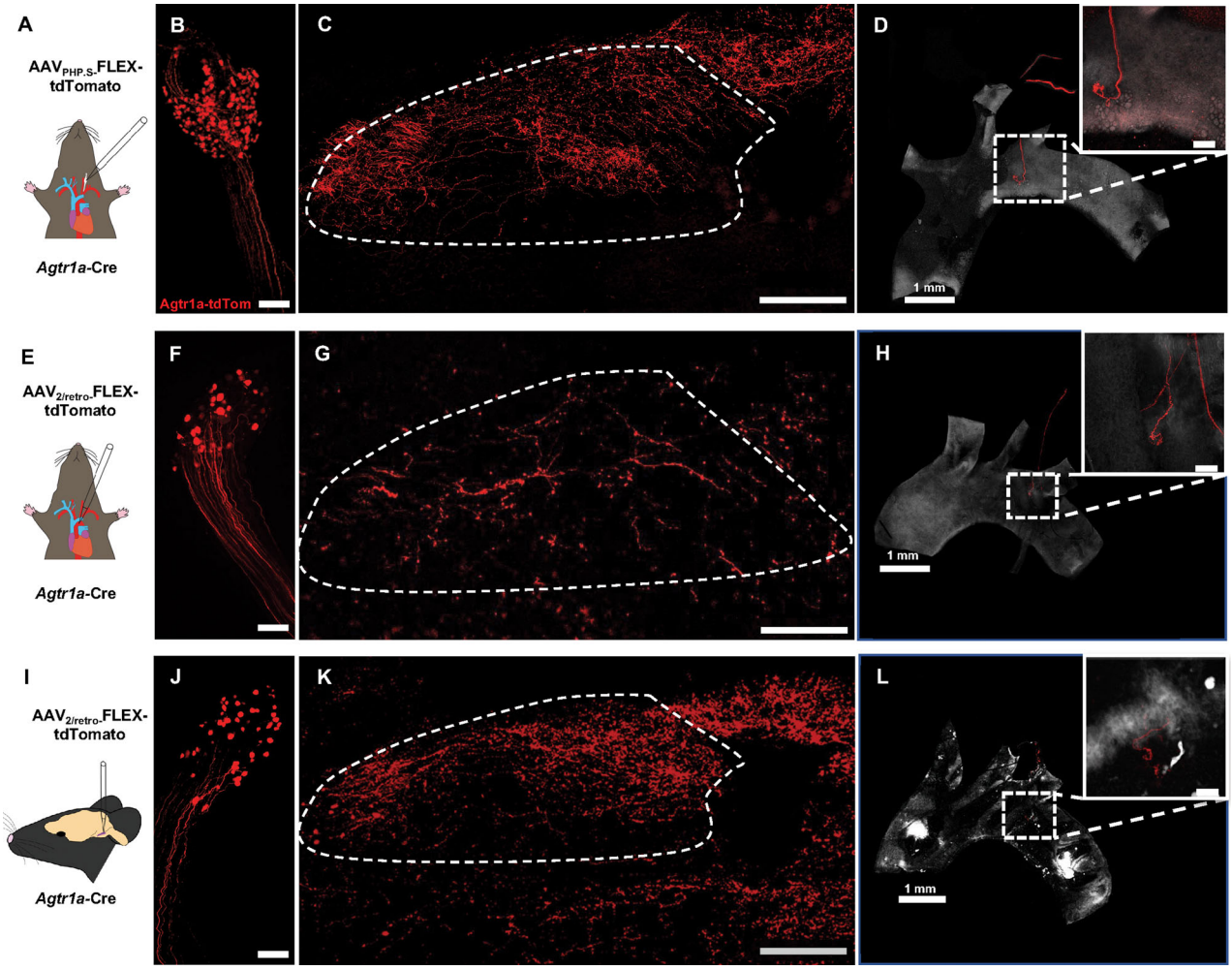

Figure 3. NG^{AT1aR} are positioned to transmit vagal sensory afferent (baroreceptor) information from the aortic arch to the NTS. ***A–D***, Anterograde Cre-inducible AAV delivered to the NG of *Agtr1a-Cre* mice induces robust expression of tdTomato in *Agtr1a*-containing (***B***) cell bodies within the NG and afferent fibers (***C***) in the caudal NTS and (***D***) the aortic arch. ***E–H***, Retrograde Cre-inducible AAV delivered to the aortic arch of *Agtr1a-Cre* mice also induces robust expression of tdTomato in *Agtr1a*-containing (***F***) cell bodies within the NG and afferent fibers innervating the (***G***) caudal NTS and (***H***) aortic arch. ***I–L***, Retrograde Cre-inducible AAV delivered to the caudal NTS of *Agtr1a-Cre* mice induces robust expression of tdTomato in *Agtr1a*-containing (***J***) cell bodies within the NG and afferent fibers innervating the (***K***) caudal NTS and (***L***) aortic arch. Scale bar = 100 µm unless stated otherwise.

transporter 2 and release the neurotransmitter, glutamate, within the NTS (Talman et al., 1980; Schaffar et al., 1997; Lachamp et al., 2006). To determine if *Agtr1a*-containing afferent input to the caudal NTS is glutamatergic, subsequent studies examined the ability of blue light to induce glutamate release from axons of AT1aR-containing neurons in the NTS by performing acute brain slice preparations in *Agtr1a-ChR2* mice. NTS neurons were targeted for electrophysiological characterization (Fig. 5*A*) and evaluated in whole-cell voltage-clamp configuration at −50 mV. Blue light pulses (1 ms) induced large excitatory synaptic currents (Fig. 5*B*) with a mean amplitude of −507.4 ± 109.1 pA ($n = 26$). Overall, 25 of 26 NTS neurons tested demonstrated a mean light-evoked current with amplitude >5 times the RMS noise observed during the baseline period. A subset of NTS neurons with large light-evoked currents were challenged with bath-applied glutamate receptor antagonists (20 µM DNQX and 40 µM AP5), which reduced light-evoked inward currents to 3.3 ± 1.1% of their baseline level ($n = 6$, $p = 3.64 \times 10^{-9}$), confirming that light-evoked excitatory currents in NTS neurons result from glutamatergic signaling (Fig. 5*C*).

Next, to evaluate the sufficiency of stimulating the afferent nerve endings in the NTS to prompt sustained reductions in BP and HR in the conscious state, *Agtr1a-ChR2* mice and control *Agtr1a-Cre* mice were implanted with radiotelemetry devices intraperitoneally and fiber-optic posts into the caudal NTS (Fig. 5*D*). As can be observed in Figure 5*E–H*, optical stimulation of these afferents in *Agtr1a-ChR2* mice produced robust decreases in all parameters (mixed-effects analysis followed by Dunnett's multiple-comparisons test). Baseline values (SBP, DBP, MAP, and HR) used to calculate Δ values in response to optical stimulation at each frequency are reported in Table 1. There was no impact of optical stimulation of the caudal NTS on any of these parameters in the *Agtr1a-Cre* control mice. Specifically, there was a significant genotype by frequency interaction for SBP ($F_{(3,39)} = 5.33$, $p = 0.0036$), MAP ($F_{(3,39)} = 6.18$, $p = 0.0003$), DBP ($F_{(3,39)} = 5.84$, $p = 0.0021$), and HR ($F_{(3,39)} = 9.30$, $p < 0.0001$; Fig. 5*E–H*). Compared to baseline, 1–3 Hz stimulation produced significant reductions in SBP, MAP, DBP, and HR (Fig. 5*E–H*). SBP, MAP, and DBP responses in *Agtr1a-ChR2* mice were significantly different from *Agtr1a-Cre* mice responses at 2–3 Hz stimulation (Fig. 5*E–G*). HR responses in *Agtr1a-ChR2* mice were significantly different from *Agtr1a-Cre* mice responses at 1–3 Hz (Fig. 5*H*). Further, linear regression analyses revealed that optical stimulation of these afferents produces

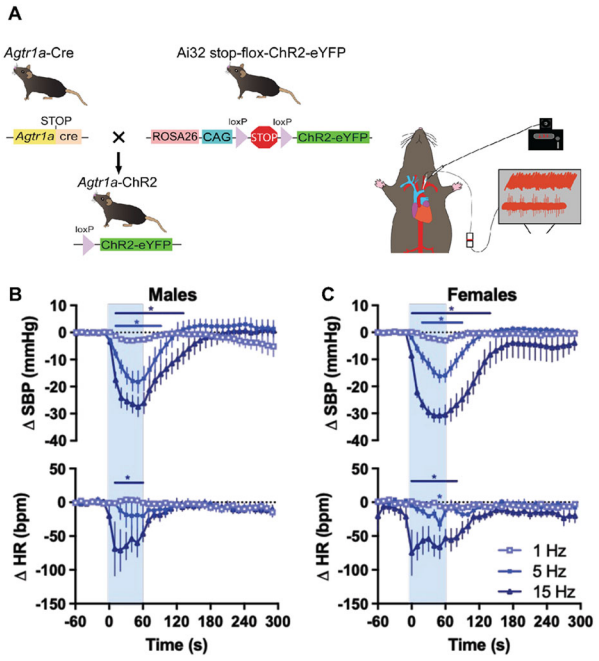

Figure 4. Optogenetic simulation of NG^{AT1aR} is sufficient to reduce BP and HR, thus recapitulating baroreflex responses. ***A***, Illustration depicting the generation of the *Agtr1a-ChR2* mouse line (left) and acute recording preparation (right). While anesthetized, male and female *Agtr1a-ChR2* (male, $n = 8$; female, $n = 5–7$) were catheterized to assess SBP and HR. Subsequently, the left NG was isolated in order to optogenetically stimulate NG^{AT1aR} neurons. ***B***,***C***, Changes in SBP and HR in (***B***) males and (***C***) females during optogenetic stimulation with different photoactivation parameters (473 nm; 1, 5, or 15 Hz; 60 s). *Significantly different from baseline (time = 0 s), $p < 0.05$, two-way RM ANOVA or mixed-effects analysis with Dunnett's multiple-comparisons test.

frequency-dependent decreases in SBP ($F_{(1,3)} = 71.78$, $p = 0.0035$), DBP ($F_{(1,3)} = 64.62$, $p = 0.004$), MAP ($F_{(1,3)} = 70.79$, $p = 0.0035$), and HR ($F_{(1,3)} = 51.38$, $p = 0.0056$; Fig. 5*E–H*). These results suggest that stimulation of *Agtr1a*-containing afferents within the caudal NTS is sufficient to elicit compensatory frequency-dependent responses to perceived changes in vascular stretch.

Agtr1a-containing afferent input within the NTS elicits patterns of c-*fos* expression that are consistent with baroreflex activation and initiation of subsequent compensatory responses

Following cardiovascular assessments, *Agtr1a-ChR2* and *Agtr1a-Cre* control mice were used to determine patterns of c-*fos* expression within the brain, in particular, to determine if optical stimulation of *Agtr1a*-containing afferents within the NTS induces a pattern of neural activation within cardiovascular control centers that is consistent with baroreflex activation and/or with the compensatory responses observed (e.g., decreases in BP and HR). That is, mice underwent another round of optical stimulation (473 nm blue light; 20 ms pulses; 2 Hz; cycles of 1 min on, followed by 1 min of rest; 60 min total duration) and then were perfused 90 min later, and brains were collected and processed for c-*fos* IHC. Quantitative analyses of these results are presented in Figure 6*A*. As expected, optical stimulation of afferents in the caudal NTS significantly increased the number of c-*fos*–positive nuclei observed within the NTS itself of *Agtr1a-ChR2* mice compared with control *Agtr1a-Cre* mice (Fig. 6*B*; $t_{(6)} = 5.19$, $p = 0.016$, unpaired *t* test), as well as other brain regions involved in cardiovascular and fluid volume regulation (Fig. 6*C*,*D*). These patterns of neural activation are consistent with baroreflex activation and initiation of subsequent compensatory responses to restore BP following increased vascular stretch (Potts et al., 1997; Chan and Sawchenko, 1998; Chan et al., 2000; Grindstaff et al., 2000).

Experimental models of hypertension alter the temporal firing patterns of NG^{AT1aR} during acute elevations in BP

A hallmark of hypertension is baroreflex insensitivity (Grassi et al., 2014; Mancia and Grassi, 2014). In particular, the DOCA–salt and Ang-II–induced experimental models of hypertension have independently been associated with increases in central and/or peripheral Ang-II and baroreflex impairment (Guo and Abboud, 1984; Nakamura et al., 1988; Ueno et al., 1988). To determine whether such elevations in BP are similarly associated with altered functionality of NG^{AT1aR}, we conducted an in vivo Ca^{2+} imaging study. The goal was to evaluate the impact of acute vasoconstriction induced by phenylephrine on the activity of NG^{AT1aR}. The *Agtr1a-GCaMP6s* mice that were used for these studies were generated by breeding *Agtr1a-Cre* mice with *Ai96 stop-flox-GCaMP6s* mice (Fig. 7*A*), an approach that is again similar to what was used to generate the *Agtr1a-tdTomato* and the *Agtr1a-ChR2* mice described above.

Agtr1a-GCaMP6s mice either remained normotensive or were subjected to the DOCA–salt or chronic Ang-II infusion models (Fig. 7*B*). After 3 weeks of exposure to these conditions, mice were used for in vivo anesthetized cardiovascular assessments (Fig. 7*C*) or two-photon intravital imaging studies (Fig. 7*D*). There was a significant effect of treatment on anesthetized baseline SBP (Fig. 7*E–G*; $F_{(2,17)} = 5.51$, $p = 0.014$; one-way ANOVA followed by Tukey's multiple-comparisons test). Anesthetized baseline SBPs for each group were higher in the DOCA–salt and Ang-II–treated mice (normotensive control mice, 78.04 ± 1.58 mmHg; DOCA–salt-treated mice, 92.99 ± 5.02 mmHg; and Ang-II–treated mice, 101.5 ± 6.81 mmHg), but phenylephrine (0.1 mg/kg, i.v.) resulted in similar relative increases in the magnitude or dynamics of the pressor responses in all groups ($F_{(24,408)} = 35.68$, $p < 0.0001$, two-way RM ANOVA followed by Tukey's multiple-comparisons test).

Two-photon intravital imaging of NG^{AT1aR} revealed that phenylephrine also significantly increased GCaMP6s fluorescence within NG^{AT1aR} in all three conditions; however, the dynamics of the responses were significantly different between the groups. That is, the increased GCaMP6s fluorescence observed after administration of phenylephrine was significantly delayed in mice that were subjected to DOCA–salt or chronic delivery of Ang-II (Fig. 7*H–P*). There was a significant time–treatment interaction (i.e., control, DOCA–salt, Ang-II) for change in GCaMP6s fluorescence ($\Delta F/F$) in response to phenylephrine ($F_{(358,21,122)} = 10.90$, $p < 0.0001$, two-way RM ANOVA followed by Sidak's multiple-comparisons test). Post hoc analyses revealed that the $\Delta F/F$ was elevated above baseline (time = 60 s) between 77 and 150 s and between 156 and 179 s for the control group, between 77 and 179 s for the DOCA–salt group, and between 85 and 179 s for the Ang-II group (Fig. 7*K–M*). The implication is that the responses are delayed in mice subjected to experimental models of hypertension. Moreover, between-subjects post hoc analyses (Sidak's multiple-comparisons test) revealed significant differences in $\Delta F/F$ between the DOCA–salt-treated and normotensive control mice, with the values being lower between 84 and 91 s, and higher between 123 and 132 s and 154 and 166 s (Fig. 7*L*). Compared to normotensive control mice, $\Delta F/F$ in Ang-II–treated mice was significantly lower between 70 and 118 s and higher between 130 and 179 s (Fig. 7*M*). Lastly, $\Delta F/F$ in response to phenylephrine in DOCA–salt-treated mice was significantly lower at 78 and 106 s

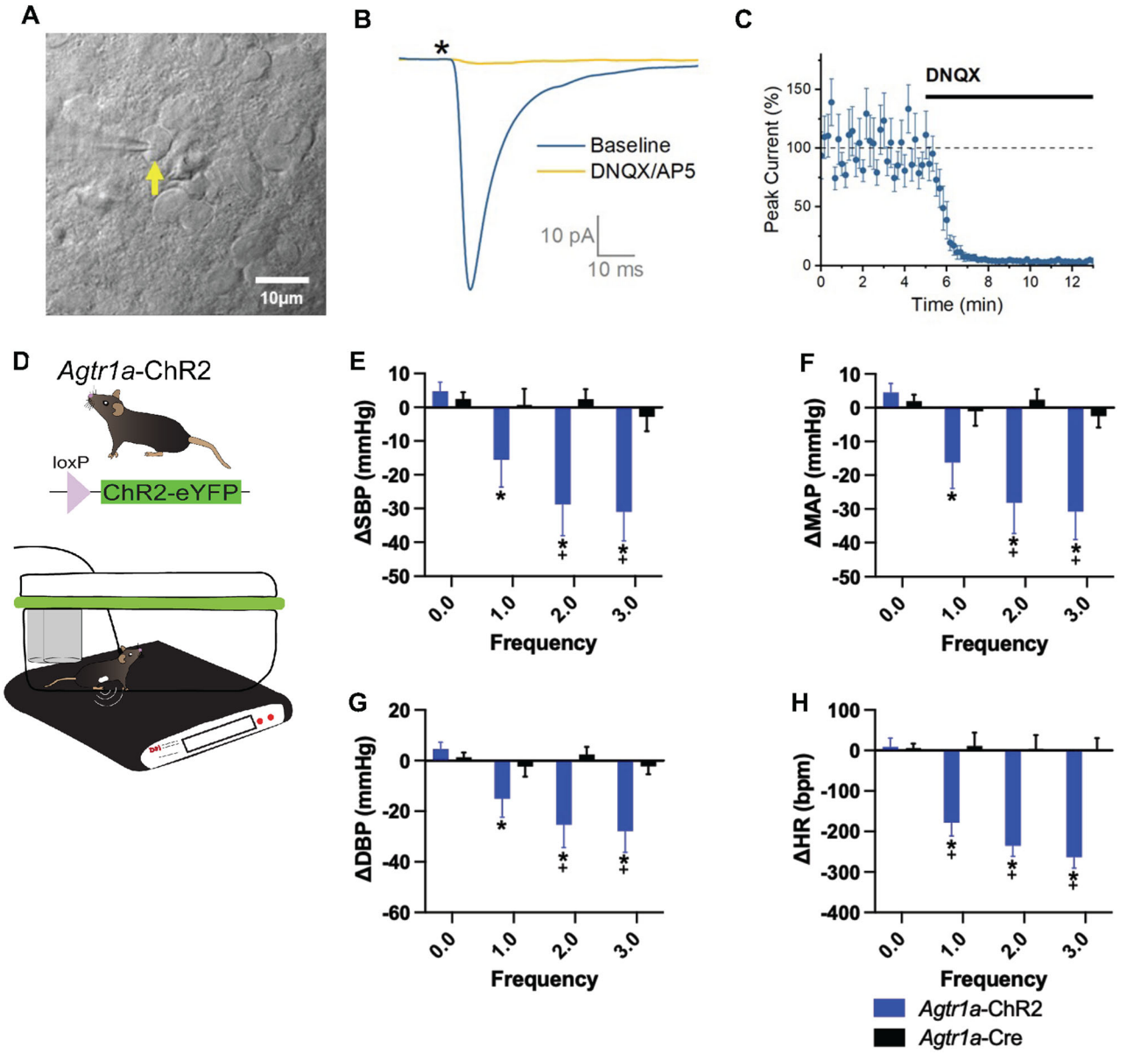

Figure 5. Optogenetic stimulation of *Agtr1a*-expressing input into the caudal NTS prompts glutamate release onto second-order neurons and causes robust frequency-dependent alterations in cardiovascular parameters. ***A***, Differential interference contrast image of in vitro NTS preparation, followed by panels showing expression of ChR2-eYFP in *Agtr1a-ChR2* mice and biocytin-filled cell patched in the NTS. ***B***,***C***, 1 ms of stimulation with blue light produced inward currents in NTS cells voltage-clamped at −70 mV in 10/11 attempts. ***B***, Mean normalized amplitude in 3/3 cells tested with bath application of ionotropic glutamate receptor antagonists and (***C***) the evoked response from a representative cell. ***D***, Illustration of *Agtr1a-ChR2* mouse and awake-behaving optical stimulation experiment setup. ***E–H***, Changes in (***E***) SBP, (***F***) MAP, (***G***) DBP, and (***H***) HR at 30 min after optical stimulation onset with different parameters (473 nm; 1, 2, or 3 Hz). *Different from baseline (frequency = 0 Hz), $p < 0.05$, mixed-effects analysis followed by Dunnett's multiple-comparisons test; $^{+}$different from control, $p < 0.05$, mixed-effects analysis followed by Sidak's multiple-comparisons test; *Agtr1a-ChR2*, $n = 7–11$; *Agtr1a-Cre*, $n = 7–9$.

and 111 and 125 s than that in Ang-II–treated mice, and higher at 135 and 179 s (Fig. 7*M*). Two-way RM ANOVA of the area under the curve [AUC; determined from $\Delta F/F$ during the baseline (1–60 s), early (61–120 s), and late (121–180 s) post-phenylephrine administration periods] revealed that there was a significant time–treatment interaction ($F_{(4,354)} = 31.98$, $p < 0.0001$). Post hoc analyses (i.e., Sidak's multiple-comparisons test) then revealed early and late post-phenylephrine responses that were elevated compared with baseline for all groups (control, DOCA–salt, and Ang-II; Fig. 7*K–M*). Between-subjects comparisons further revealed that, while there were no differences among the groups during the baseline period, AUC of $\Delta F/F$ responses of the DOCA–salt-treated mice and Ang-II–treated mice were significantly lower than normotensive control mice during the early post-phenylephrine phase but were significantly higher during the late post-phenylephrine phase. Lastly, compared with DOCA–salt-treated mice, Ang-II–treated mice exhibited blunted $\Delta F/F$ AUC responses during the early post-phenylephrine phase, while they were significantly higher at the late post-phenylephrine phase. The implication is that the responsivity of NG^{AT1R} to the acute pressor challenge is delayed in mice given DOCA–salt, and this effect is exacerbated in the Ang-II mice. Collectively, the delayed responses to phenylephrine that we observed indicate that chronically elevated BP may impair baroreflex sensitivity by shifting temporal patterns by which NG^{AT1aR} fire action potentials in response to acute hypertensive challenges.

Table 1. Average baseline values (mean ± SEM) for *Agtr1a*-ChR2 ($n = 7–11$) and *Agtr1a*-Cre ($n = 8–13$) mice

	0 Hz		1 Hz		2 Hz		3 Hz	
	Agtr1a-ChR2	*Agtr1a-Cre*	*Agtr1a-ChR2*	*Agtr1a-Cre*	*Agtr1a-ChR2*	*Agtr1a-Cre*	*Agtr1a-ChR2*	*Agtr1a-Cre*
SBP (mmHg)	96.95 ± 2.46	100.27 ± 2.09	100.04 ± 2.38	105.44 ± 3.13	100.70 ± 1.99	105.36 ± 2.10	100.20 ± 2.40	104.08 ± 3.51
DBP (mmHg)	71.25 ± 1.61	74.73 ± 2.34	74.57 ± 3.13	81.06 ± 2.38	75.69 ± 3.08	80.69 ± 2.09	75.17 ± 2.94	81.06 ± 2.38
MAP (mmHg)	84.69 ± 1.95	87.40 ± 2.46	87.86 ± 2.78	93.36 ± 2.99	88.78 ± 2.48	93.18 ± 2.08	88.25 ± 2.58	91.77 ± 3.98
HR (bpm)	440.33 ± 15.66	459.50 ± 15.16	457.61 ± 31.01	443.88 ± 23.33	474.10 ± 20.45	483.58 ± 31.20	476.47 ± 22.64	411.49 ± 52.16

Baseline values used to calculate Δ values in response to optical stimulation at each frequency tested.

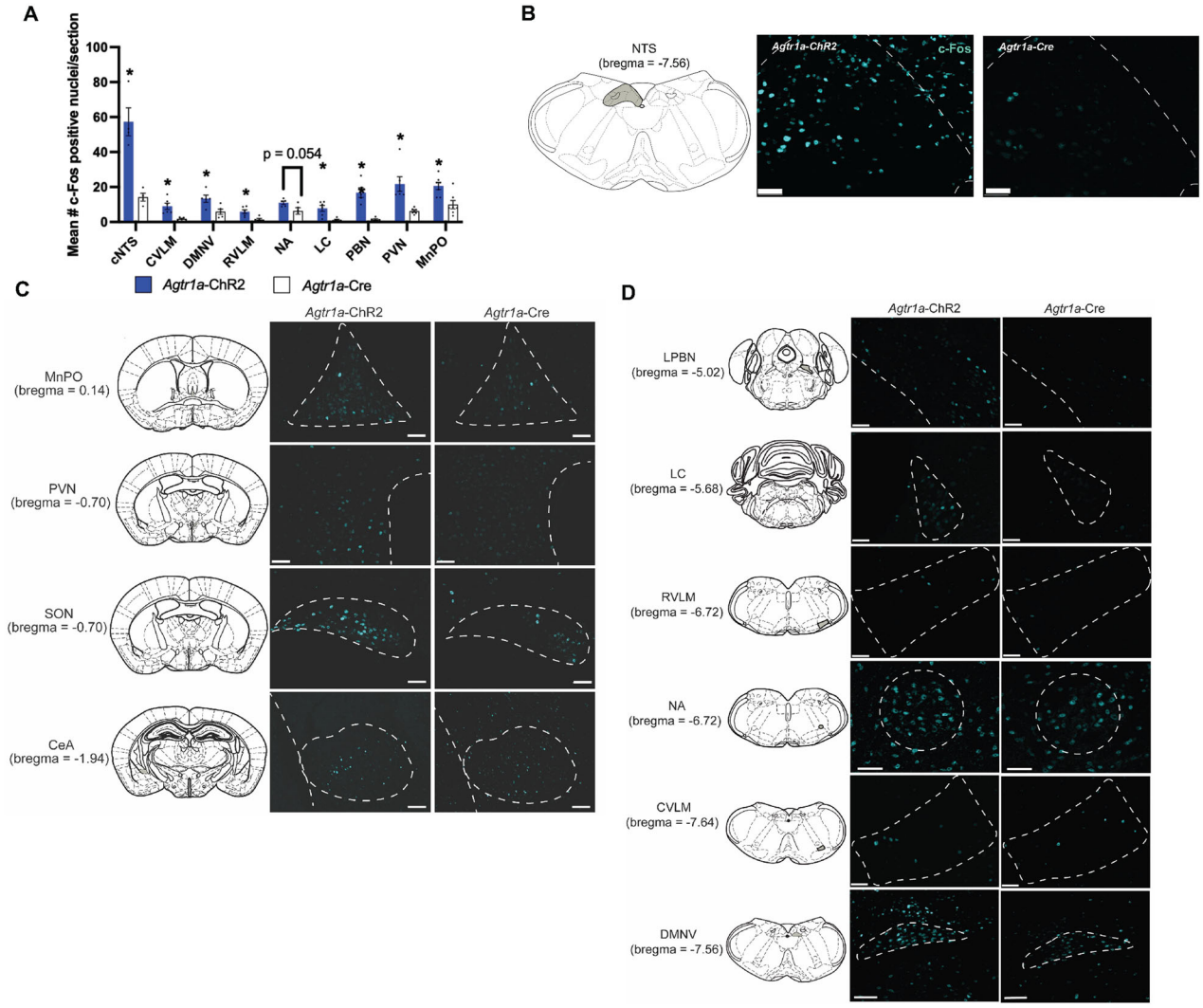

Figure 6. Optical stimulation of *Agtr1a*-containing input into the caudal NTS prompts neural activation in key cardioregulatory areas of the brain. ***A***, Quantification of c-*fos* positive nuclei in forebrain and hindbrain cardioregulatory regions. *Significant difference between *Agtr1a-ChR2* and *Agtr1a-Cre* mice, $p < 0.05$, multiple unpaired *t* tests. *p*-value noted above regions in which there was not a significant difference between *Agtr1a-ChR2* and *Agtr1a-Cre* mice. ***B***, Representative images of c-*fos* expression in caudal NTS of *Agtr1a-ChR2* mouse and *Agtr1a-Cre* mouse. (***B***) Scale bar = 50 µm. ***C***,***D***, Representative images from *Agtr1a-ChR2* and *Agtr1a-Cre* mice reflecting c-*fos* expression within the (***C***) forebrain and (***D***) hindbrain areas following optical stimulation. CeA, central nucleus of the amygdala; CVLM, caudal ventrolateral medulla; DMNV, dorsal motor nucleus of the vagus; LPBN, lateral parabrachial nucleus; LC, locus coeruleus; MnPO, median preoptic nucleus; NA, nucleus ambiguus; PVN, paraventricular nucleus of the hypothalamus; RVLM, rostral ventrolateral medulla; SON, supraoptic nucleus. All images were acquired at 20× magnification, except CeA acquired at 10× magnification. (***C***,***D***) Scale bar = 50 µm.

Optical stimulation of *Agtr1a*-containing afferent input within the NTS circumvents baroreflex impairment in DOCA–salt-treated conscious freely moving male mice

We next hypothesized that these NG^{AT1aR} neurons remain therapeutic targets for hypertension, despite their altered dynamics in responsivity to baroreflex stimulation. In other words, we predicted that optical stimulation of NG^{AT1aR} afferent input within the NTS would circumvent this baroreflex insensitivity observed when subjected to a chronic hypertensive stimulus. To test this, *Agtr1a-ChR2* mice and *Agtr1a-Cre* controls were implanted with telemetry devices and subjected to optical excitation while normotensive and following DOCA–salt treatment (Fig. 8*A*). Data from baseline and experimental cardiovascular recordings were assessed between ∼11:00 A.M. and ∼3:00 P.M. (Fig. 8*B*). DOCA–salt

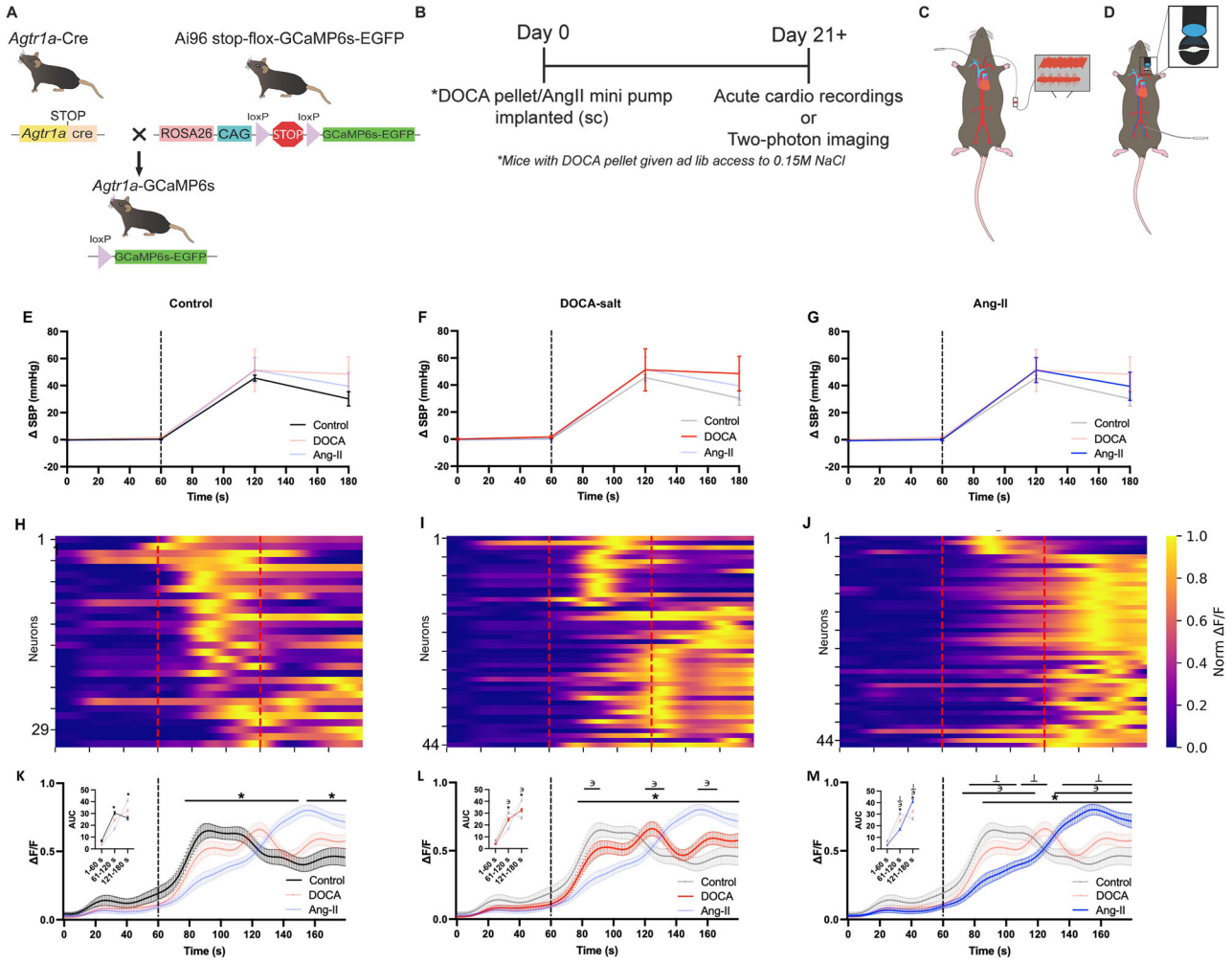

Figure 7. Models of increased BP are associated with altered dynamics of calcium responses in NG^{AT1aR}. ***A***, Illustration depicting the generation of *Agtr1a-GCaMP6s* mice. ***B***, Experimental timeline. ***C***, While anesthetized, male *Agtr1a-GCaMP6s* mice were catheterized to (***D***) assess SBP in response to intravenous phenylephrine (control, $n = 7$; DOCA, $n = 5$; Ang-II, $n = 8$) or (***E***) perform two-photon intravital imaging while recording changes in GCaMP6s fluorescence from NG^{AT1aR} in response to intravenous phenylephrine (control, $n = 4$; DOCA, $n = 5$; Ang-II, $n = 3$). ***E–G***, Graphs depicting a change in SBP (ΔSBP) to intravenous phenylephrine administration (0.1 mg/kg; denoted by a dashed line at time = 60 s) in (***E***) control ($n = 7$), (***F***) DOCA-treated ($n = 5$), and (***G***) Ang-II–treated ($n = 3$) *Agtr1a-GCaMP6s* mice. ***H–J***, Heat maps of the fluorescence signal (Δ*F*/*F*) from individual NG^{AT1aR} 60 s before, during, and after intravenous phenylephrine administration (0.1 mg/kg; denoted by red dashed lines at time = 60 s and time = 120 s) in (***H***) control ($n = 29$ neurons), (***I***) DOCA-treated ($n = 44$ neurons), and (***J***) Ang-II–treated mice ($n = 45$ neurons). Each row represents the mean activity for a single neuron. ***K–M***, Graphs of mean fluorescence signal (Δ*F*/*F*) and AUC of mean fluorescence signal from NG^{AT1aR} in response to intravenous phenylephrine administration (0.1 mg/kg; denoted by a dashed line at time = 60 s) in (***K***) control, (***L***) DOCA-treated, and (***M***) Ang-II–treated mice. *Significantly different from baseline (time = 60 s), $p < 0.05$; ∋Significantly different from control, $p < 0.05$; ⊥Significantly different from DOCA, $p < 0.05$, two-way RM ANOVA followed by Sidak's multiple-comparisons tests.

treatment led to a modest increase in baseline (normotensive) SBP compared with their pretreatment SBP in both *Agtr1a-ChR2* mice and *Agtr1a-Cre* mice (Table 2). Two-way RM ANOVAs revealed the minimal impact of optical stimulation (473 nm, 2 Hz, 1 min on/off for 60 min) within the caudal NTS of *Agtr1a-Cre* control mice on MAP, SBP, and HR during normotensive or DOCA–salt conditions (Fig. 8*C–E*). On the other hand, such analyses revealed significant time–group interactions for these parameters in *Agtr1a-ChR2* mice subjected to the same optical stimulation paradigm [SBP ($F_{(24,144)} = 8.32$, $p < 0.0001$), MAP ($F_{(24,144)} = 8.97$, $p < 0.0001$), and HR ($F_{(24,144)} = 19.90$, $p < 0.0001$)]. Figure 8, *C–H*, highlights the robust decreases in MAP, SBP, and HR in response to optical stimulation within the caudal NTS of *Agtr1a-ChR2* in both normotensive and DOCA–salt conditions, as well as the results of post hoc analyses indicating that, compared with baseline (time = 0 min), normotensive *Agtr1a-ChR2* mice exhibit significant decreases in SBP between 10 and 80 min and at 190 min, MAP between 10 and 80 min and at 150 min and 190 min, and HR between 10 and 90 min, between 140 and 160 min, and at 190 min. Also compared with baseline (time = 0), *Agtr1a-ChR2* mice given DOCA–salt exhibited significant decreases in SBP between 10 and 170 min and at 240 min, MAP between 10 and 170 min, at 200 min and at 240 min, and HR between 10 and 70 min, between 150 and 170 min, at 200 min and at 240 min. Finally, when comparing normotensive versus DOCA–salt conditions, depressor responses in *Agtr1a-ChR2* mice were significantly blunted in magnitude early on (i.e., 20–60 min for SBP; 30–60 min for MAP) but enhanced later (i.e., 90–130 min and at 240 min for SBP; at 100 min, 120 min, and 240 min for MAP). Bradycardic responses are similarly blunted at 70 min, 90 min, and 180 min. Thus, cardiovascular responses were prolonged following DOCA–salt treatment (Fig. 8*F–H*), suggesting enhanced benefit. The collective implication is that optical stimulation of *Agtr1a*-containing afferent input to the caudal NTS causes robust decreases in BP and HR in awake freely moving mice under both normotensive and DOCA–salt conditions.

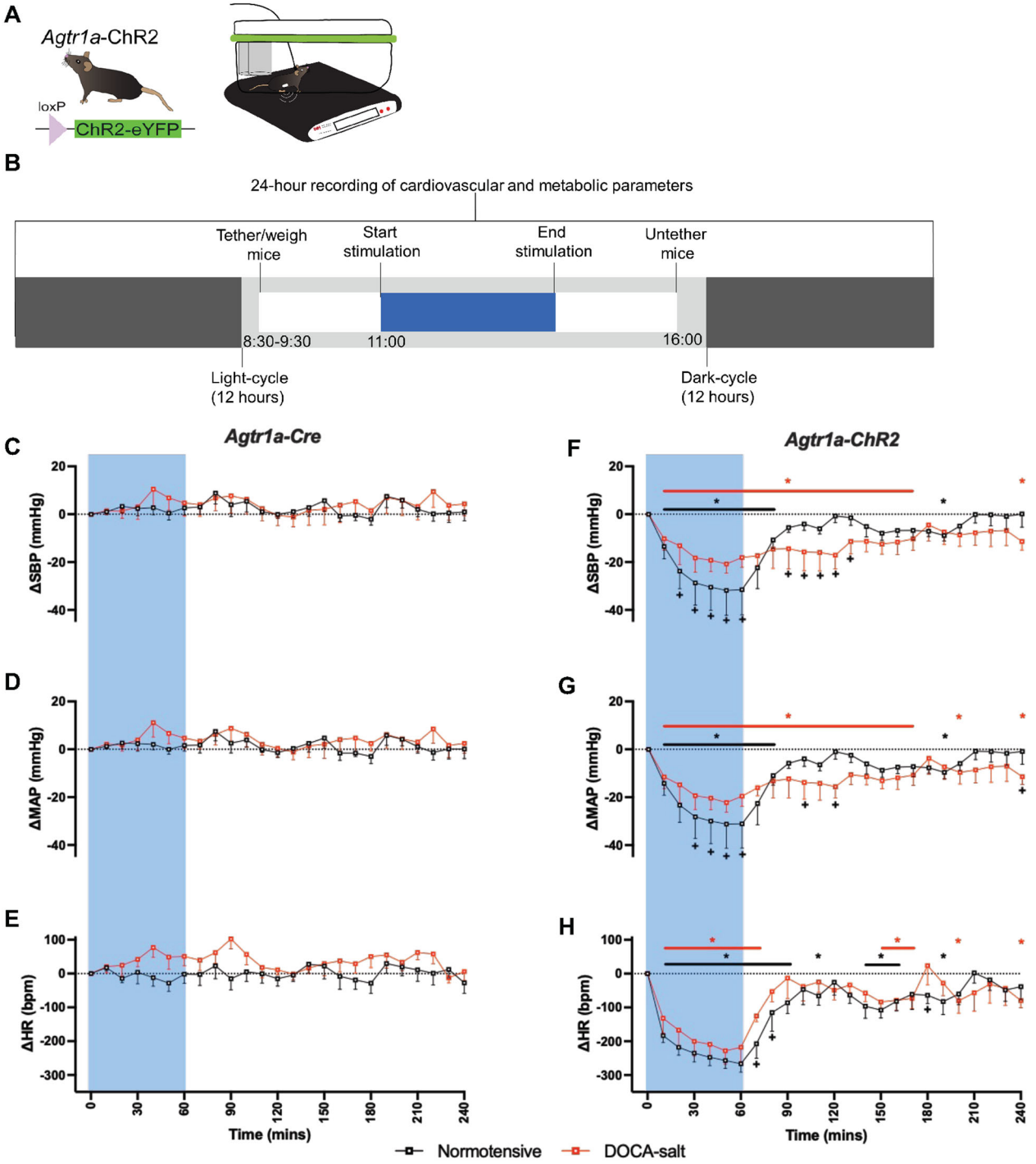

Figure 8. Optical stimulation of *Agtr1a*-containing afferents within the NTS produces robust decreases in cardiovascular parameters in normotensive and DOCA–salt-treated mice. Effects of optogenetic activation (20 ms pulses, 2 Hz, 1 min on followed by 1 min off, 60 min) of *Agtr1a*-expressing afferent input into the caudal NTS on cardiovascular parameters. ***A***, Schematic depicting *Agtr1a-ChR2* mouse line and fiber-optic targeting caudal NTS. ***B***, Experimental timeline. ***C–H***, Effects of activation under normotensive conditions and DOCA–salt conditions in (***C–E***) *Agtr1a-Cre* and (***F–H***) *Agtr1a-ChR2* mice. The error bars indicate SEM. *Significantly different from baseline (time = 0 min), $p < 0.05$, two-way RM ANOVA followed by uncorrected Fisher's LSD multiple-comparisons test + significantly different from *Agtr1a-Cre*-light ON, $p < 0.05$, two-way RM ANOVA followed by uncorrected Fisher's LSD multiple-comparisons test; *Agtr1a-ChR2*, $n = 7–11$; *Agtr1a-Cre*, $n = 8–9$.

Discussion

These studies used a multifaceted approach to reveal the structure and cardiovascular-related function of a specific angiotensin-sensitive neural circuit that serves as a point of convergence between the endocrine (RAAS) and neural (vagal afferent) regulation of BP. The key findings include the identification of a subset of NG neurons expressing *Agtr1a*, rendering them sensitive to Ang-II (Rhaleb et al., 1991; Ito et al., 1995; Matsumura et al., 1998). Additionally, some of these NG^{AT1aR} neuronal afferents are ideally positioned in the aortic arch to relay sensory information about vascular stretch to the NTS. Excitation of the NG^{AT1aR} pathway induces compensatory neural and cardiovascular responses associated with baroreflex activation in response to increased vascular stretch. Importantly, even during conditions that are associated

Table 2. Average normotensive and DOCA–salt-treated baseline values (mean ± SEM) for *Agtr1a-ChR2* ($n = 7–11$) and *Agtr1a-Cre* ($n = 8–13$) mice

	Normotensive		DOCA–salt	
	Agtr1a-ChR2	*Agtr1a-Cre*	*Agtr1a-ChR2*	*Agtr1a-Cre*
SBP (mmHg)	100.61 ± 1.27	104.37 ± 2.09	114.86 ± 2.64*	119.75 ± 1.05*
DBP (mmHg)	74.61 ± 1.42	77.93 ± 2.25	86.33 ± 1.42*	90.18 ± 1.86*
MAP (mmHg)	88.08 ± 1.19	91.10 ± 2.40	100.62 ± 2.38*	104.30 ± 1.34*
HR (bpm)	453.67 ± 11.64	474.69 ± 8.36	417.53 ± 10.14*	407.55 ± 6.22*

There was a significant effect of DOCA–salt treatment for SBP ($F_{(1,13)} = 56.71$, $p < 0.0001$), DBP ($F_{(1,13)} = 62.29$, $p < 0.0001$), MAP ($F_{(1,13)} = 60.56$, $p < 0.0001$), and HR ($F_{(1,13)} = 54.95$, $p < 0.0001$); two-way RM ANOVA followed by Bonferroni's multiple-comparisons test.
*Significantly different from within group normotensive value ($p < 0.05$).

with high BP, this pathway remains a viable target for reducing BP and HR.

Cardiovascular homeostasis involves the integration of endocrine signals with vagal afferent input from arterial baroreceptors within the CNS. The overall idea that this integration occurs at the level of the NG^{AT1aR} is novel. Ang-II acts on AT1R(s) located throughout the brain and body to impact autonomic, endocrine, and behavioral factors to maintain BP (Gehlert et al., 1984; Mendelsohn et al., 1984; McKinley et al., 2003) and our data, along with previous studies (Kupari et al., 2019), highlight the presence of *Agtr1*a(s) within a subset of NG neurons. Our anatomical studies extend these findings by revealing that NG^{AT1aR} are positioned to communicate sensory information pertaining to vascular stretch from the aortic arch to the brain, forming the so-called aortic claws (Min et al., 2019). The present studies also reveal that a subset of NG^{AT1aR} expresses *Piezo1/2*, which are mechanosensitive channels that are implicated in the sensation of vascular stretch and BP regulation (Zeng et al., 2018; Elsaafien et al., 2022). However, it is important to acknowledge that parallel studies also uncovered some NG^{AT1aR} innervation elsewhere (e.g., carotid sinus, GI tract, esophagus) and a substantial proportion of NG^{AT1aR} do not express *Piezo1/2*, suggesting a diverse impact on physiology. Further, these NG^{AT1aR} are, as a whole, distinct from the *Piezo1/2*-containing afferents studied by Zeng et al. (2018) and Min et al. (2019).

Baroreceptor afferents have the ability to modify cardiovascular parameters in a frequency-dependent manner, increasing firing frequency in response to the magnitude of vascular stretch and inducing compensatory responses (Miles, 1986; Mifflin and Felder, 1988; Scheuer et al., 1996). These studies are the first to indicate that optogenetic excitation of NG^{AT1aR} soma or *Agtr1a*-containing afferent input within the NTS produces robust frequency-dependent decreases in BP and HR. These responses align with those produced by pharmacological baroreflex activation (Estañol et al., 2011; Iliescu et al., 2014; Yao et al., 2022) or by electrical stimulation of the aortic depressor nerve (De Paula et al., 1999). Additionally, baroreceptor afferent signaling is dependent on glutamate release in the NTS (Talman et al., 1980; Sykes et al., 1997). Electrophysiological studies confirm that optical excitation of *Agtr1a*-containing afferents within the NTS results in glutamate release onto postsynaptic (non-*Agtr1a*-containing) neurons. Using c-*fos* as a marker of neural activation, we determined that optical excitation of *Agtr1a*-containing afferent input within the NTS produced a pattern of activation consistent with previous studies that pharmacologically or surgically manipulated baroreceptor signaling and, subsequently, evaluated c-*fos* expression (Chan and Sawchenko, 1998; Chan et al., 2000; Grindstaff et al., 2000). Collectively, these results suggest that NG^{AT1aR} anatomically look and function similar to baroreceptive afferents.

Another novel finding of these studies is that two models of mildly elevated BP (DOCA–salt and Ang-II infusion), both of which have been associated with baroreflex impairment and increased brain Ang-II levels (Veelken et al., 1994; Xia et al., 2013), exhibit altered dynamics of NG^{AT1aR} responses to pressor stimuli. Functionally, there is evidence that Ang-II may act at NG^{AT1aR} to blunt arterial baroreflex sensitivity (Zhang et al., 2010; Li and Zheng, 2011). A potential mechanism for this impairment is the downregulation of *Piezo1/2*, the expression of which is lower in Ang-II–induced hypertension (Huo et al., 2021). However, there is also evidence that Ang-II causes depolarization of rat isolated NG neurons (Widdop et al., 1992), suggesting that it may stimulate baroreflex responses. Thus, the role that NG^{AT1aR} and/or Ang-II binding to AT1aR on NG neurons plays in the development of hypertension remains unclear. Here, Ca^{2+} imaging of NG^{AT1aR} revealed, for the first time, that DOCA–salt and Ang-II treatment delayed the responsivity of these neurons to changes in BP induced by phenylephrine, suggesting that these hypertensive models impair NG^{AT1aR}'s ability to sense changes in vascular stretch.

We then sought to determine if optical excitation of *Agtr1a*-containing afferent input within the NTS could overcome this impairment in baroreflex sensitivity in DOCA–salt hypertension. These studies revealed that targeting *Agtr1a*-containing afferent input recapitulates the robust decreases in BP and HR observed in the normotensive condition. Much like the altered dynamics of responsivity of the NG^{AT1aR} during DOCA–salt, the depressor and bradycardic responses were also altered during DOCA–salt. That is, in the DOCA–salt condition, decreases in BP and HR were attenuated in magnitude early on but were sustained for a longer duration overall. The implication is that these neurons are responding later and staying active longer, consistent with the results from intravital Ca^{2+} imaging experiments. Thus, NG^{AT1aR} stimulation can overcome baroreceptor impairment when BP is elevated and could be a potential target to alleviate it.

There are some limitations of the present study. While it characterizes *Agtr1a* as a phenotypic marker of NG neurons involved in cardiovascular regulation, the precise localization or function of the receptor (AT1aR) on NG afferents remains unclear. Previous binding studies provide some insight in this regard, by highlighting bidirectional transport of AT1R(s) along the vagus nerve (Diz and Ferrario, 1988) and showing binding sites localized to the NG, throughout the vagus, and at the terminals both within the NTS and at the target organs (Allen et al., 1988). Future experiments manipulating AT1aR expression on these afferents may provide more insight into the role of the receptor. Additionally, there are notable sex differences in baroreflex function (Salman et al., 2020), and the sensitivity of the baroreflex also varies across the estrus cycle (Pamidimukkala et al., 2003; Goldman et al., 2009), such that during stages of the estrus cycle in which levels of estrogen and progesterone are elevated (e.g., mid-luteal phase), baroreflex sensitivity is increased. Further, there are several lines of evidence highlighting estrogen–Ang-II receptor interactions (Nickenig et al., 1998; Kisley et al., 1999; Krause et al., 2007). While our studies reveal that male and female mice respond similarly to optogenetic stimulation of NG^{AT1aR}, we do not consider the impact of the stage of the estrus cycle on these effects, nor do we evaluate the impact of DOCA–salt on these responses in female mice. Future studies should expand on the findings presented here to determine the effect of chronic stimulation in females.

Another important consideration is that some studies use *Agtr1a-tdTomato*, *Agtr1a-ChR2*, or *Agtr1a-GCaMP6s* knock-in

mice to evaluate the structure and function of this pathway. These approaches lead to the expression of tdTomato, ChR2, or GCaMP6s in cells that synthesize *Agtr1a* at any point in development and may result in transient gene expression in cells that no longer express *Agtr1a*. While ISH demonstrates a high degree of colocalization between *Agtr1a* mRNA and tdTomato expression, the presence of tdTomato neurons that don't express *Agtr1a* mRNA may be explained by permanent loxP recombination resulting from transient Cre expression. Future functional studies with enhanced specificity might provide additional insight. Finally, some experiments examine cardiovascular function during optogenetic stimulation within the NTS of male *Agtr1a*-ChR2 mice and controls, thus targeting all *Agtr1a*-expressing afferents and soma within the NTS. However, the abundance of AT1R binding sites within the NTS predominantly arises from the NG, as unilateral ablation of the NG eliminated the binding in the ipsilateral NTS (Speth et al., 1987).

From a clinical perspective, modulation of the baroreflex to treat hypertension has been considered a therapeutic option for many decades; however, the success of this approach has been limited (Schwartz et al., 1967; Rothfeld et al., 1969; Gierthmuehlen et al., 2020; Lauder et al., 2020; Mahfoud et al., 2021). Pharmacological manipulation of the RAAS has been more successful in treating hypertension (Atlas, 2007; Mentz et al., 2013). However, many patients do not have their BP under control, emphasizing the need for novel targets and therapeutics. Current device-based baroreflex activation therapeutics exclusively target carotid sinus baroreceptors, which transmit sensory information to the brainstem by way of the petrosal ganglia. This study introduces a novel approach, targeting a subset of baroreceptor afferents that are distinct from those targeted clinically (i.e., those that express *Agtr1a* are localized to the NG and that sense stretch within the aortic arch). These NG^{AT1aR} act as an integrative site for neural (baroreceptor) and endocrine (Ang-II) signals pertaining to changes in blood volume and pressure. Notably, they are sufficient to sense and initiate the appropriate compensatory responses to such changes in both normotensive and hypertensive conditions. The collective overall implication is that these NG^{AT1aR} may be exploited as a novel route to understand and alleviate hypertension.

References

Allen AM, McKinley MJ, Oldfield BJ, Dampney RA, Mendelsohn FA (1988) Angiotensin II receptor binding and the baroreflex pathway. Clin Exp Hypertens A 10:63–78.

Armstrong M, Kerndt CC, Moore RA (2022) *StatPearls*. Treasure Island, FL: StatPearls Publishing LLC.

Atlas SA (2007) The renin–angiotensin aldosterone system: pathophysiological role and pharmacologic inhibition. J Manag Care Pharm 13:9–20.

Bai L, et al. (2019) Genetic identification of vagal sensory neurons that control feeding. Cell 179:1129–1143.e3.

Berthoud HR, Neuhuber WL (2000) Functional and chemical anatomy of the afferent vagal system. Auton Neurosci 85:1–17.

Bevegard BS, Shepherd JT (1966) Circulatory effects of stimulating the carotid arterial stretch receptors in man at rest and during exercise. J Clin Invest 45:132–142.

Brierley DI, et al. (2020) Central and peripheral GLP-1 systems independently and additively suppress eating. bioRxiv:2020.2008.2003.234427.

Brown AM (1980) Receptors under pressure. An update on baroreceptors. Circ Res 46:1–10.

Chan RK, Jarvina EV, Sawchenko PE (2000) Effects of selective sinoaortic denervations on phenylephrine-induced activational responses in the nucleus of the solitary tract. Neuroscience 101:165–178.

Chan RK, Sawchenko PE (1998) Organization and transmitter specificity of medullary neurons activated by sustained hypertension: implications for understanding baroreceptor reflex circuitry. J Neurosci 18:371–387.

Cunningham JT, Wachtel RE, Abboud FM (1995) Mechanosensitive currents in putative aortic baroreceptor neurons in vitro. J Neurophysiol 73:2094–2098.

de Kloet AD, et al. (2017) A unique "angiotensin-sensitive" neuronal population coordinates neuroendocrine, cardiovascular, and behavioral responses to stress. J Neurosci 37:3478–3490.

de Kloet AD, Wang L, Ludin JA, Smith JA, Pioquinto DJ, Hiller H, Steckelings UM, Scheuer DA, Sumners C, Krause EG (2016) Reporter mouse strain provides a novel look at angiotensin type-2 receptor distribution in the central nervous system. Brain Struct Funct 221:891–912.

de Leeuw PW, Alnima T, Lovett E, Sica D, Bisognano J, Haller H, Kroon AA (2015) Bilateral or unilateral stimulation for baroreflex activation therapy. Hypertension 65:187–192.

de Leeuw PW, Bisognano JD, Bakris GL, Nadim MK, Haller H, Kroon AA, DEBuT-HT, Rheos Trial I (2017) Sustained reduction of blood pressure with baroreceptor activation therapy: results of the 6-year open follow-up. Hypertension 69:836–843.

De Paula PM, Castania JA, Bonagamba LG, Salgado HC, Machado BH (1999) Hemodynamic responses to electrical stimulation of the aortic depressor nerve in awake rats. Am J Physiol 277:R31–R38.

Diz DI, Barnes KL, Ferrario CM (1986) Contribution of the vagus nerve to angiotensin II binding sites in the canine medulla. Brain Res Bull 17:497–505.

Diz DI, Ferrario CM (1988) Bidirectional transport of angiotensin II binding sites in the vagus nerve. Hypertension 11:I139–143.

Elsaafien K, Harden SW, Johnson DN, Kimball AK, Sheng W, Smith JA, Scott KA, Frazier CJ, de Kloet AD, Krause EG (2022) A novel organ-specific approach to selectively target sensory afferents innervating the aortic arch. Front Physiol 13:841078.

Elsaafien K, Kirchner MK, Mohammed M, Eikenberry SA, West C, Scott KA, de Kloet AD, Stern JE, Krause EG (2021) Identification of novel cross-talk between the neuroendocrine and autonomic stress axes controlling blood pressure. J Neurosci 41:4641–4657.

Epstein SE, Beiser GD, Goldstein RE, Stampfer M, Wechsler AS, Glick G, Braunwald E (1969) Circulatory effects of electrical stimulation of the carotid sinus nerves in man. Circulation 40:269–276.

Estañol B, Porras-Betancourt M, Padilla-Leyva M, Sentíes-Madrid H (2011) A brief history of the baroreceptor reflex: from Claude Bernard to Arthur C. Guyton. Illustrated with some classical experiments. Arch Cardiol Mex 81:330–336.

Fitzsimons JT (1998) Angiotensin, thirst, and sodium appetite. Physiol Rev 78:583–686.

Gabriel M, Seller H (1970) Interaction of baroreceptor afferents from carotid sinus and aorta at the nucleus tractus solitarii. Pflugers Arch 318:7–20.

Gehlert DR, Speth RC, Healy DP, Wamsley JK (1984) Autoradiographic localization of angiotensin II receptors in the rat brainstem. Life Sci 34:1565–1571.

Gierthmuehlen M, Plachta DTT, Zentner J (2020) Implant-mediated therapy of arterial hypertension. Curr Hypertens Rep 22:16.

Giovannucci A, et al. (2019) CaImAn an open source tool for scalable calcium imaging data analysis. Elife 8:e38173.

Goldman RK, Azar AS, Mulvaney JM, Hinojosa-Laborde C, Haywood JR, Brooks VL (2009) Baroreflex sensitivity varies during the rat estrous cycle: role of gonadal steroids. Am J Physiol Regul Integr Comp Physiol 296:R1419–1426.

Grassi G, Seravalle G, Brambilla G, Pini C, Alimento M, Facchetti R, Spaziani D, Cuspidi C, Mancia G (2014) Marked sympathetic activation and baroreflex dysfunction in true resistant hypertension. Int J Cardiol 177:1020–1025.

Grindstaff RJ, Grindstaff RR, Sullivan MJ, Cunningham JT (2000) Role of the locus ceruleus in baroreceptor regulation of supraoptic vasopressin neurons in the rat. Am J Physiol Regul Integr Comp Physiol 279:R306–R319.

Guo GB, Abboud FM (1984) Angiotensin II attenuates baroreflex control of heart rate and sympathetic activity. Am J Physiol 246:H80–H89.

Han W, et al. (2018) A neural circuit for gut-induced reward. Cell 175:887–888.

Healy DP, Rettig R, Nguyen T, Printz MP (1989) Quantitative autoradiography of angiotensin II receptors in the rat solitary-vagal area: effects of nodose ganglionectomy or sinoaortic denervation. Brain Res 484:1–12.

Huo L, et al. (2021) Piezo2 channel in nodose ganglia neurons is essential in controlling hypertension in a pathway regulated directly by Nedd4-2. Pharmacol Res 164:105391.

Iliescu R, Tudorancea I, Lohmeier TE (2014) Baroreflex activation: from mechanisms to therapy for cardiovascular disease. Curr Hypertens Rep 16:453.

Isaacson JS, Reid IA (1990) Importance of endogenous angiotensin II in the cardiovascular responses to sympathetic stimulation in conscious rabbits. Circ Res 66:662–671.

Ito M, Oliverio MI, Mannon PJ, Best CF, Maeda N, Smithies O, Coffman TM (1995) Regulation of blood pressure by the type 1A angiotensin II receptor gene. Proc Natl Acad Sci U S A 92:3521–3525.

Kisley LR, Sakai RR, Fluharty SJ (1999) Estrogen decreases hypothalamic angiotensin II AT1 receptor binding and mRNA in the female rat. Brain Res 844:34–42.

Krause EG, Curtis KS, Markle JP, Contreras RJ (2007) Oestrogen affects the cardiovascular and central responses to isoproterenol of female rats. J Physiol 582:435–447.

Kupari J, Haring M, Agirre E, Castelo-Branco G, Ernfors P (2019) An atlas of vagal sensory neurons and their molecular specialization. Cell Rep 27: 2508–2523.e4.

Lachamp P, Crest M, Kessler JP (2006) Vesicular glutamate transporters type 1 and 2 expression in axon terminals of the rat nucleus of the solitary tract. Neuroscience 137:73–81.

Lanfranchi PA, Somers VK (2002) Arterial baroreflex function and cardiovascular variability: interactions and implications. Am J Physiol Regul Integr Comp Physiol 283:R815–826.

Lauder L, Azizi M, Kirtane AJ, Bohm M, Mahfoud F (2020) Device-based therapies for arterial hypertension. Nat Rev Cardiol 17:614–628.

Li H, Weatherford ET, Davis DR, Keen HL, Grobe JL, Daugherty A, Cassis LA, Allen AM, Sigmund CD (2011) Renal proximal tubule angiotensin AT1A receptors regulate blood pressure. Am J Physiol Regul Integr Comp Physiol 301:R1067–R1077.

Li YL, Zheng H (2011) Angiotensin II-NADPH oxidase-derived superoxide mediates diabetes-attenuated cell excitability of aortic baroreceptor neurons. Am J Physiol Cell Physiol 301:C1368–C1377.

Lohmeier TE, Dwyer TM, Hildebrandt DA, Irwin ED, Rossing MA, Serdar DJ, Kieval RS (2005) Influence of prolonged baroreflex activation on arterial pressure in angiotensin hypertension. Hypertension 46:1194–1200.

Mahfoud F, Schlaich MP, Lobo MD (2021) Device therapy of hypertension. Circ Res 128:1080–1099.

Mancia G, Grassi G (2014) The autonomic nervous system and hypertension. Circ Res 114:1804–1814.

Matsumura K, Averill DB, Ferrario CM (1998) Angiotensin II acts at AT1 receptors in the nucleus of the solitary tract to attenuate the baroreceptor reflex. Am J Physiol 275:R1611–R1619.

McKinley MJ, McAllen RM, Davern P, Giles ME, Penschow J, Sunn N, Uschakov A, Oldfield BJ (2003) The sensory circumventricular organs of the mammalian brain. Adv Anat Embryol Cell Biol 172:III–XII, 1–122, back cover.

Mendelsohn FA, Quirion R, Saavedra JM, Aguilera G, Catt KJ (1984) Autoradiographic localization of angiotensin II receptors in rat brain. Proc Natl Acad Sci U S A 81:1575–1579.

Mentz RJ, et al. (2013) The past, present and future of renin–angiotensin aldosterone system inhibition. Int J Cardiol 167:1677–1687.

Mifflin SW, Felder RB (1988) An intracellular study of time-dependent cardiovascular afferent interactions in nucleus tractus solitarius. J Neurophysiol 59:1798–1813.

Miles R (1986) Frequency dependence of synaptic transmission in nucleus of the solitary tract in vitro. J Neurophysiol 55:1076–1090.

Min S, Chang RB, Prescott SL, Beeler B, Joshi NR, Strochlic DE, Liberles SD (2019) Arterial baroreceptors sense blood pressure through decorated aortic claws. Cell Rep 29:2192–2201.e3.

Mohammed M, et al. (2022) Targeting angiotensin type-2 receptors located on pressor neurons in the nucleus of the solitary tract to relieve hypertension in mice. Cardiovasc Res 118:883–896.

Morimoto S, Cassell MD, Sigmund CD (2002) Glia- and neuron-specific expression of the renin–angiotensin system in brain alters blood pressure, water intake, and salt preference. J Biol Chem 277:33235–33241.

Nakamura Y, Takeda K, Nakata T, Hayashi J, Kawasaki S, Lee LC, Sasaki S, Nakagawa M, Ijichi H (1988) Central attenuation of aortic baroreceptor reflex in prehypertensive DOCA–salt-loaded rats. Hypertension 12:259–266.

Nickenig G, et al. (1998) Estrogen modulates AT1 receptor gene expression in vitro and in vivo. Circulation 97:2197–2201.

Paintal AS (1973) Vagal sensory receptors and their reflex effects. Physiol Rev 53:159–227.

Paintal AS (1977) Thoracic receptors connected with sensation. Br Med Bull 33:169–174.

Pamidimukkala J, Taylor JA, Welshons WV, Lubahn DB, Hay M (2003) Estrogen modulation of baroreflex function in conscious mice. Am J Physiol Regul Integr Comp Physiol 284:R983–R989.

Potts PD, Polson JW, Hirooka Y, Dampney RA (1997) Effects of sinoaortic denervation on Fos expression in the brain evoked by hypertension and hypotension in conscious rabbits. Neuroscience 77:503–520.

Rhaleb NE, Rouissi N, Nantel F, D'Orleans-Juste P, Regoli D (1991) Dup 753 is a specific antagonist for the angiotensin receptor. Hypertension 17:480–484.

Rothfeld EL, Parsonnet V, Raman KV, Zucker IR, Tiu R (1969) The effect of carotid sinus nerve stimulation on cardiovascular dynamics in man. Angiology 20:213–218.

Salman IM, Ameer OZ, McMurray S, Giarola AS, Sridhar A, Lewis SJ, Hsieh YH (2020) Laterality influences central integration of baroreceptor afferent input in male and female Sprague Dawley rats. Front Physiol 11:499.

Schadt JC, Ludbrook J (1991) Hemodynamic and neurohumoral responses to acute hypovolemia in conscious mammals. Am J Physiol 260:H305–H318.

Schaffar N, Rao H, Kessler JP, Jean A (1997) Immunohistochemical detection of glutamate in rat vagal sensory neurons. Brain Res 778:302–308.

Scheffers IJ, et al. (2010) Novel baroreflex activation therapy in resistant hypertension: results of a European multi-center feasibility study. J Am Coll Cardiol 56:1254–1258.

Scherrer U, Pryor SL, Bertocci LA, Victor RG (1990) Arterial baroreflex buffering of sympathetic activation during exercise-induced elevations in arterial pressure. J Clin Invest 86:1855–1861.

Scheuer DA, Zhang J, Toney GM, Mifflin SW (1996) Temporal processing of aortic nerve evoked activity in the nucleus of the solitary tract. J Neurophysiol 76:3750–3757.

Schwartz SI, Griffith LS, Neistadt A, Hagfors N (1967) Chronic carotid sinus nerve stimulation in the treatment of essential hypertension. Am J Surg 114:5–15.

Speth RC, Dinh TT, Ritter S (1987) Nodose ganglionectomy reduces angiotensin II receptor binding in the rat brainstem. Peptides 8:677–685.

Sumners C, et al. (2020) Brain angiotensin type-1 and type-2 receptors: cellular locations under normal and hypertensive conditions. Hypertens Res 43:281–295.

Sykes RM, Spyer KM, Izzo PN (1997) Demonstration of glutamate immunoreactivity in vagal sensory afferents in the nucleus tractus solitarius of the rat. Brain Res 762:1–11.

Talman WT, Perrone MH, Reis DJ (1980) Evidence for L-glutamate as the neurotransmitter of baroreceptor afferent nerve fibers. Science 209: 813–815.

Ueno Y, Mohara O, Brosnihan KB, Ferrario CM (1988) Characteristics of hormonal and neurogenic mechanisms of deoxycorticosterone-induced hypertension. Hypertension 11:I172–177.

Veelken R, Hilgers KF, Ditting T, Leonard M, Mann JF, Geiger H, Luft FC (1994) Impaired cardiovascular reflexes precede deoxycorticosterone acetate–salt hypertension. Hypertension 24:564–570.

Wallbach M, Born E, Kampfer D, Luders S, Muller GA, Wachter R, Koziolek MJ (2020) Long-term effects of baroreflex activation therapy: 2-year follow-up data of the BAT neo system. Clin Res Cardiol 109:513–522.

Wehrwein EA, Joyner MJ (2013) Regulation of blood pressure by the arterial baroreflex and autonomic nervous system. Handb Clin Neurol 117:89–102.

Widdop RE, Krstew E, Jarrott B (1992) Electrophysiological responses of angiotensin peptides on the rat isolated nodose ganglion. Clin Exp Hypertens A 14:597–613.

Xia H, Sriramula S, Chhabra KH, Lazartigues E (2013) Brain angiotensin-converting enzyme type 2 shedding contributes to the development of neurogenic hypertension. Circ Res 113:1087–1096.

Yao Y, et al. (2022) Cardiovascular baroreflex circuit moonlights in sleep control. Neuron 110:3986–3999.e6.

Zeng WZ, Marshall KL, Min S, Daou I, Chapleau MW, Abboud FM, Liberles SD, Patapoutian A (2018) PIEZOs mediate neuronal sensing of blood pressure and the baroreceptor reflex. Science 362:464–467.

Zhang L, Tu H, Li YL (2010) Angiotensin II enhances hyperpolarization-activated currents in rat aortic baroreceptor neurons: involvement of superoxide. Am J Physiol Cell Physiol 298:C98–C106.

Zhao Q, Yu CD, Wang R, Xu QJ, Dai Pra R, Zhang L, Chang RB (2022) A multidimensional coding architecture of the vagal interoceptive system. Nature 603:878–884.